JOURNAL OF GEOPHYSICAL RESEARCH, VOL. 112, B07302, doi:10.1029/2006JB004717, 2007

Conditions governing the occurrence of supershear ruptures under slip-weakening friction

Eric M. Dunham[1]

Received 25 August 2006; revised 13 December 2006; accepted 27 March 2007; published 4 July 2007.

[1] A general theory for transitions between sub-Rayleigh and intersonic rupture speeds is developed for faults governed by slip-weakening friction. The transition occurs when stresses moving at intersonic speeds ahead of expanding or accelerating sub-Rayleigh ruptures exceed the peak strength of the fault, initiating slip within a daughter crack. Upon reaching a critical nucleation length, the daughter crack becomes dynamically unstable, expanding into a self-sustaining intersonic rupture. This mechanism holds in both two and three dimensions. On faults with uniform properties, the seismic S ratio $[S = (\tau_p - \tau_0)/(\tau_0 - \tau_r)]$, a measure of the initial loading stress, τ_0, relative to the peak and residual strengths, τ_p and τ_r, respectively, must be smaller than some critical value for the transition to occur. The maximum S value for unbounded faults in three dimensions is 1.19, smaller than the value of 1.77 that Andrews (1985) has shown to govern the transition in two dimensions. The supershear transition length (i.e., how far the rupture propagates before reaching intersonic speeds) is proportional to a length scale arising from the friction law governing the nucleation and stability of the daughter crack. A sufficiently narrow fault width suppresses the transition; the critical width is approximately 0.8 times the transition length on an unbounded fault. The transition length is highly sensitive to the form of the slip-weakening law even when the associated fracture energies are identical. Heterogeneous propagation, in the form of abrupt accelerations or increases in stress-release rate, induces stress-wave radiation that can trigger transient bursts of intersonic propagation.

Citation: Dunham, E. M. (2007), Conditions governing the occurrence of supershear ruptures under slip-weakening friction, *J. Geophys. Res.*, *112*, B07302, doi:10.1029/2006JB004717.

1. Introduction

[2] Recognition of the influence of rupture directivity on strong ground motion has prompted a move to incorporate the effect in seismic hazard analysis. Current efforts, however, have focused on parameterizing the effects of directivity only for subshear ruptures [*Somerville et al.*, 1997; *Spudich et al.*, 2004]. At the same time, there is a growing body of evidence that shows that ruptures can and often do propagate at intersonic speeds [*Archuleta*, 1984; *Spudich and Cranswick*, 1984; *Bouchon et al.*, 2000, 2001, 2002; *Bouchon and Vallée*, 2003; *Ellsworth et al.*, 2004; *Dunham and Archuleta*, 2004]. Since directivity results from the interference of waves radiated from each point on a fault, it is consequently determined by the timing, or propagation velocity, of the rupture. A pronounced manifestation of this is the difference between ground motions of sub-Rayleigh and intersonic ruptures; in the latter, radiating S waves constructively coalesce into a Mach front that transports large velocities, accelerations, and stresses far from the fault [*Bernard and Baumont*, 2005; *Dunham and Archuleta*, 2005; *Bhat et al.*, 2007]. The resulting directivity pattern is profoundly altered [*Aagaard and Heaton*, 2004].

[3] Given the essential need to understand if, when, and where supershear earthquakes might strike, many have turned to rupture dynamics in hopes of gaining an understanding of the conditions which give rise to supershear earthquakes. This problem has a lengthy history, beginning with both theoretical and numerical models [*Burridge*, 1973; *Andrews*, 1976; *Das and Aki*, 1977; *Burridge et al.*, 1979]. More recently, the supershear transition has been explored numerically in three dimensions [*Day*, 1982b; *Madariaga and Olsen*, 2000; *Madariaga et al.*, 2000; *Fukuyama and Olsen*, 2002; *Dunham et al.*, 2003]. A complementary approach has been taken in laboratory fracture experiments. Initially, these involved crack growth initiated by impact loading [*Rosakis et al.*, 1999], and finite-element analyses [*Needleman*, 1999] provided much insight into the observed phenomena. A more recent set of experiments was conducted under conditions bearing far more similarity to ruptures on natural faults [*Xia et al.*, 2004]. Despite the growing body of literature on the problem, no consensus exists regarding the basic mechanics of the supershear transition, and no single theory has been shown to govern the observed phenomenology in both two and three dimensions. This work aims to bridge these studies and, by conducting a detailed examination of the physical

[1]Department of Earth and Planetary Sciences, Harvard University, Cambridge, Massachusetts, USA.

0148-0227/07/2006JB004717$09.00

processes occurring during the supershear transition, to provide a unifying framework to describe the transition in various geometries. This permits us to address such issues as requisite stress levels needed to initiate supershear propagation and the existence of minimum propagation distances before the supershear transition is achieved.

[4] The early numerical experiments of *Andrews* [1976] and *Das and Aki* [1977] on two-dimensional mode-II cracks demonstrated that, for a given stress level, expanding ruptures begin in the sub-Rayleigh regime and accelerate toward the Rayleigh speed. If the initial stress exceeds a critical level, a peak in shear stress traveling at the S wave speed, first identified by *Burridge* [1973], initiates slip ahead of the main rupture in what has been termed the daughter crack. The daughter crack eventually becomes unstable, and the rupture jumps to an intersonic speed. The parameter determining whether or not a daughter crack forms is the background level of initial loading, τ_0, relative to the peak and residual strengths, τ_p and τ_r, respectively, quantified in terms of the nondimensional seismic S ratio: $S = (\tau_p - \tau_0)/(\tau_0 - \tau_r)$ [*Andrews*, 1976; *Das and Aki*, 1977]. Their numerical results further quantified how far the main rupture must propagate before the supershear transition occurs, relative to another length scale in the problem: the Griffith crack length for singular cracks in elastostatic equilibrium. In a laboratory investigation of ruptures along frictionally held interfaces, *Xia et al.* [2004] have qualitatively reproduced the behavior observed in the numerical models. The dependence of the transition length on the loading level differed from that obtained by *Andrews* [1976]; they attributed this discrepancy to variation of one of the frictional parameters (the slip-weakening distance) with normal stress. Upon introducing such a dependence, their results fell into much closer agreement with those of Andrews.

[5] From a different perspective, this work identifies several complications regarding the equations of motion of a crack tip, i.e., predicting the trajectory of a rupture in response to variations in fracture energy or stress drop. Derivation of a crack-tip equation of motion was one of the classic quests of dynamic fracture mechanics, reaching a successful culmination in the work of *Kostrov* [1966, 1975], *Eshelby* [1969], and *Freund* [1972a, 1972b]; the development is well summarized by *Freund* [1998, chap. 7]. All of these studies were limited to the sub-Rayleigh regime although recently, *Obrezanova and Willis* [2003] and *Antipov et al.* [2004] have developed approximate equations of motion for the intersonic regime in the small-scale-yielding limit, primarily to study the stability of steady intersonic propagation.

[6] An important study of the supershear transition was conducted by *Gao et al.* [2001] to explain the molecular dynamics simulations of *Abraham and Gao* [2000]. In the simulations, a block of material was loaded at its boundaries with a constant strain rate, eventually leading to crack nucleation from a preexisting slit along a weak interface. The continuum analysis of *Gao et al.* [2001] is similar in spirit to that taken in this work, in that a series of self-similar solutions are derived to approximate the stress field in front of a propagating sub-Rayleigh crack. For the particular loading studied, there is a stress peak at the S wave speed, but one which continuously grows in time (even for constant rupture speeds). The authors then proposed that as soon as the stress at this location exceeds a failure criterion, chosen to mimic that used in the simulations, then the rupture transitions to an intersonic speed. One of the main points of the current work is that, in addition to the formation of a daughter crack, the supershear transition requires that the daughter crack becomes dynamically unstable by reaching a critical length. Viewed from this perspective, transitions between sub-Rayleigh and intersonic speeds have much in common with rupture nucleation processes.

[7] The development of a theory for the supershear transition has two ingredients: a description of the rupture history prior to the transition, from which stress conditions on the fault ahead of sub-Rayleigh rupture are obtained, and an application of a friction law, which governs the development and stability of the intersonic daughter crack. The primary focus of this work is on the first of these ingredients, for which definitive conclusions and scaling laws regarding the formation (but not stability) of an intersonic daughter crack can be made without making any assumptions regarding the operative friction law. This is supplemented with a numerical demonstration of the sensitivity of the stability of the daughter crack (and its implications for predicting supershear transition lengths or durations of transient supershear bursts) to the assumed friction law.

2. General Concepts

2.1. Importance of Nonsteady Rupture Processes

[8] Rupture speed is determined by how rapidly elastic waves transmit stress changes from the slipping portion of the fault to the unweakened region ahead of the propagating rupture front. Mathematical solutions for steadily propagating ruptures exist at all speeds, but for mode-II ruptures, only those in the sub-Rayleigh and intersonic regimes have the necessary feature that energy is dissipated at the rupture front. Steady state conditions have further been shown [*Freund*, 1998, pp. 170–175] to asymptotically describe the fields surrounding any nonsteady rupture, provided that certain small-scale-yielding conditions are met. The question arises as to how a mode-II rupture, initially traveling at a sub-Rayleigh speed, can bypass the forbidden zone between the Rayleigh and S wave speed. The wavefield of ruptures propagating under steady state conditions is composed entirely of waves having fault-parallel phase velocities equal to the rupture speed; driving stresses are transmitted along the fault at exactly this speed as well. For the supershear transition to be initiated, stresses must be transmitted ahead of the rupture front at speeds at or in excess of the S wave speed. The generation of such waves requires a nonsteady rupture process, i.e., one that is a function not only of $x - vt$ but also of both/either x and/or t as well. Examples of these nonsteady rupture processes are ruptures (either of crack or pulse form) that nucleate and expand with time, initially steady ruptures that undergo rapid acceleration or encounter regions of increased stress drop, or any combination thereof. Many of these situations can be idealized to self-similar models that permit quantitative analysis; other situations require numerical solutions. Note that even self-similar ruptures (for which the rupture velocity is constant) are nonsteady in the context described

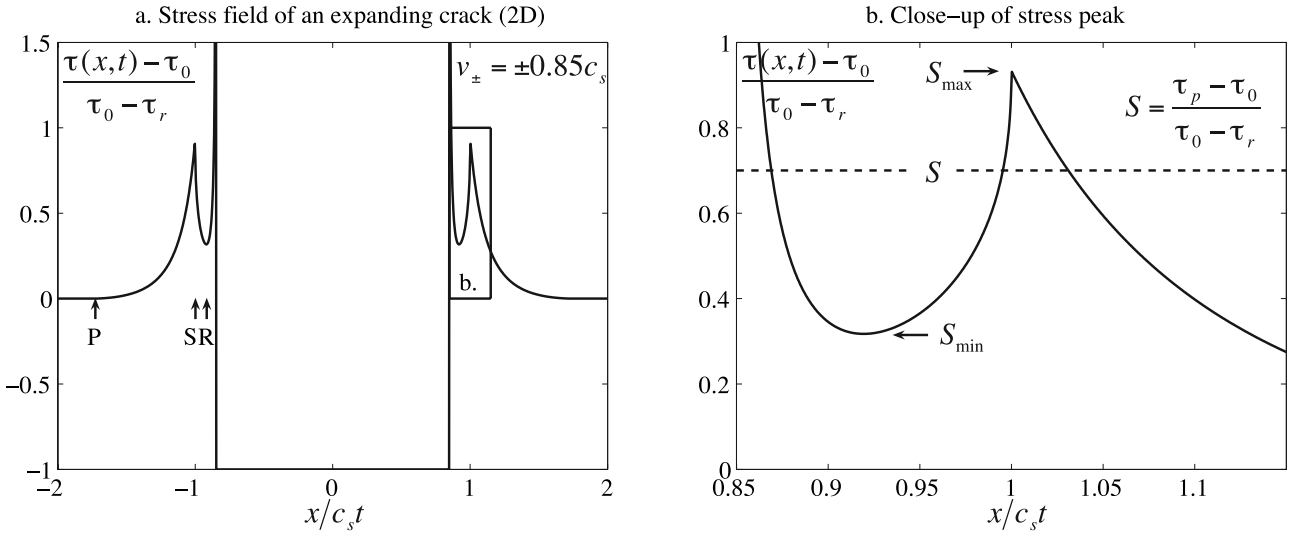

Figure 1. (a) Stress field surrounding a self-similarly expanding sub-Rayleigh rupture, with arrows marking the arrival of the *P*, *S*, and Rayleigh waves. (b) Close-up of the region near the *S* wave stress peak. Imposing a peak strength, τ_p, (nondimensionally a value of the seismic *S* ratio, appearing graphically as a horizontal dashed line on this plot) forces the growth of a daughter crack. The length of the daughter crack, L_{dc}, can be estimated as the extent of the region for which $\tau(x, t) > \tau_p$. Formation of the daughter crack occurs only when $S < S_{max}$; S_{max} is associated with the maximum value of $\tau(x, t)$ propagating at the *S* wave speed. S_{min} is similar value associated with the level of the local minimum between the main rupture front and the daughter crack.

above; their wavefields consist of waves propagating with a spectrum of phase velocities.

[9] In this work, time and distance will be measured from the point of departure from steady conditions (either from nucleation, before which the medium is at rest, or from the perturbation of initially steady propagation). The process will be centered on $(x, t) = (0, 0)$, and the length of the sub-Rayleigh main rupture, as measured from the origin, is denoted as *L*. Throughout this work, the ruptures are taken to occur within an infinite homogeneous elastic medium split by a planar fault at $y = 0$. The medium is linear elastic and is characterized by its shear modulus μ and *P* and *S* wave speeds c_p and c_s, respectively. The Rayleigh wave speed is c_R, and all results are for Poisson solids. Slip is constrained to the *x* direction, such that a mode-II rupture propagates along the *x* axis.

[10] As stated before, this work focuses on simple examples of nonsteady rupture processes. In developing quantitative models of the supershear transition, the rupture velocity after $t = 0$ but prior to the transition is taken to be constant. The rate of stress release on the fault then depends on the spatial distribution of the stress field that the rupture encounters and negates, as well as any variations in the residual strength of the fault. The change in stress may either be constant, as is the case for expanding ruptures with a constant stress drop, or may decay as some power of distance from $x = 0$. Since ruptures ultimately redistribute stress on the fault (releasing it within the rupture and loading the surrounding locked regions), the rate of stress release determines the time dependence of the amplitude of any stress waves appearing ahead of the propagating rupture (which might trigger supershear growth). If the rate of stress release is constant, then the amplitude of the stress field ahead of the rupture remains constant in time. If the rate of stress release decreases, then the stress-wave loading is transient and decays as some power of time.

2.2. Formation of Daughter Crack

[11] As a first example, consider the case of a mode-II rupture expanding bilaterally from a point at a constant sub-Rayleigh speed leaving behind it a constant stress drop, the self-similar crack model of *Burridge* [1973]. Figure 1a shows the stress field on the fault, $\tau(x, t)$, with the initial stress, τ_0, subtracted out, and the resulting change in stress due to slip, $\tau(x, t) - \tau_0$, appropriately nondimensionalized. The nondimensionalization will be specific to each problem; for the example shown, it is simply the stress drop, $\tau_0 - \tau_r$. In a later case, in which the supershear transition is initiated by stress waves induced by a jump in rupture speed from steady state propagation with a constant dynamic stress intensity factor *K*, stress will be nondimensionalized by $K/\sqrt{2\pi c_s t}$, a time-dependent factor. Despite these differences, the stress profile is rather universal, a consequence of the transient response of an elastic medium to slip on a planar fault. Stress on the fault begins to rise with the arrival of the *P* wave and reaches a maximum just prior to the arrival of the *S* wave. This feature will be referred to as the *S* wave stress peak although this terminology is perhaps misleading. At the arrival of the *S* wave, stress rapidly decreases, then it rises again until the arrival of the rupture front; the shear wavefront actually carries a rapid decrease in stress.

[12] Figure 1b takes a closer view of the region surrounding the *S* wave stress peak. Realistic friction laws bound stress to a peak strength, τ_p (in the expanding rupture example, this is expressed nondimensionally as the seismic *S* ratio). Stresses attempting to exceed this level are relaxed

by slip to form an intersonic daughter crack ahead of the sub-Rayleigh rupture. The length of the daughter crack is denoted as L_{dc}. Self-similarity implies that all lengths in the problem, including L_{dc}, grow linearly in time. The daughter crack deposits in its wake a trail of slipped and then relocked (and likely weakened) fault material into which the main rupture propagates. Furthermore, as originally postulated by *Burridge* [1973] and subsequently confirmed numerically by *Andrews* [1976], there exists a value of S, denoted in this work by S_{max}, above which the supershear transition does not occur; this is the local maximum of $[\tau(x, t) - \tau_0]/[\tau_0 - \tau_r]$ at the S wave stress peak. Finally, a consideration of the stress profile suggests the existence of another critical stress level, here termed as S_{min}, that identifies the minimum stress level (in this example propagating at the Rayleigh speed although this is not a universal feature of these solutions). For $S < S_{min}$, the peak strength level falls below the local minimum between the sub-Rayleigh rupture front and the local maximum at the S wave stress peak. In this case, one might speculate that instead of the actively slipping region being separated into a sub-Rayleigh main rupture and an intersonic daughter crack, there would be but a single slipping region with tips propagating at an intersonic speed. This may not actually be the case, however. Self-similar solutions for intersonically expanding ruptures [*Burridge*, 1973; *Broberg*, 1994, 1995] feature a logarithmic singularity in slip velocity (the logarithm arising from principal value integration across the Rayleigh pole in analytical expressions) associated with a Rayleigh interface wave. This singularity is associated with a region of negative slip velocity, which, for frictional cracks, likely corresponds to a locked region. It seems possible that such a weak singularity might be smeared out by heterogeneities in the rupture process, but numerical simulations of intersonic ruptures do reveal a locked region propagating between the Rayleigh and S wave speeds, at least for relatively smooth rupture processes. A further issue is that, by allowing slip within a daughter crack, the stress field ahead of the main rupture would be partially relaxed, likely lowering the stress level at the local minimum. Thus, using the condition $S < S_{min}$ to predict that rupture should take the form of a purely intersonic crack instead of a sub-Rayleigh crack and an intersonic daughter crack separated by a locked region should, at best, be interpreted qualitatively.

2.3. Stability of Daughter Crack

[13] The growth and stability of the daughter crack depends upon two factors: the stress ahead of the propagating rupture, which drives its expansion, and the friction law that determines the evolution and development of slip within the daughter crack. Several studies of rupture nucleation shed light upon the type of instability occurring within the daughter crack, but all have the limitation of being directly applicable only to quasi-statically growing cracks. Studies by *Campillo and Ionescu* [1997] and *Favreau et al.* [1999], later generalized by *Uenishi and Rice* [2003], examined the stability of cracks developing under slip-weakening conditions. This class of laws, in addition to having a finite peak strength, τ_p, is characterized by a weakening rate that describes the decrease in strength τ_{st} with increasing slip Δu. Quasi-static crack growth becomes unstable when the crack length exceeds a critical length that is proportional to μ/w_{sw}, where the slip-weakening rate is defined as $w_{sw} = [\partial\tau_{st}(\Delta u)/\partial u]_{\Delta u = 0}$, and in the case of a linear slip-weakening law is simply $(\tau_p - \tau_r)/D_c$, where D_c is the slip-weakening distance. The main difference between these studies, even if extended to the case of a load moving at a constant speed, and the situation encountered here is that the growth of the daughter crack occurs over a range of speeds rather than at one particular speed (say, the S wave speed).

[14] Perhaps more relevant to earthquakes are other forms of weakening. When interpreted within the framework of a power law slip-weakening model, seismic data suggest a continual weakening with slip, with the best-fitting power law exponent being about 0.3 [*Abercrombie and Rice*, 2005]. Compared to the commonly used linear slip-weakening law, this form exhibits much faster weakening at small slip. The implications of such a rapid weakening rate is discussed in sections 5 and 7.

[15] The purpose of this study is to demonstrate that the simple condition of the daughter crack reaching a critical length determines when ruptures become supershear. The rupture history generates the stress conditions ahead of the rupture front, driving the development of the daughter crack in a manner that can be quantified in terms of the daughter crack length. Coupled with a specific friction law that determines the critical daughter crack length required for nucleation, L_{nuc}, a supershear transition criterion can be formulated.

2.4. Supershear Transition Criterion

[16] The specific application of this idea is demonstrated for expanding ruptures. An estimate of the daughter crack length, nondimensionalized by $c_s t$ and denoted as $\Lambda_{dc}(S)$, is first obtained as a function of S:

$$L_{dc}/c_s t = \Lambda_{dc}(S), \tag{1}$$

which holds for all L less than the transition length (in general, S is to be replaced by the appropriately nondimensionalized peak strength, which is time-dependent in certain circumstances). The explicit scaling of the daughter crack length with time implies that the rupture process is strictly self-similar. In the event that the rupture accelerates during its growth, rather than always propagating at a constant velocity, $\Lambda_{dc}(S)$ will also depend on time. This is only the case when an additional parameter containing dimensions of length is introduced, as this is required for a proper nondimensionalization of the problem. An example would be the fracture energy controlling the growth of the main, sub-Rayleigh rupture front (which, when combined with a strength drop scale and the elastic moduli, yields a length scale). This parameter controls the rate at which ruptures accelerate [*Kostrov*, 1966].

[17] Application of a specific friction law yields an estimate of the nucleation length, L_{nuc}, of the form

$$L_{nuc}/L_{fric} = \Lambda_{nuc}(S), \tag{2}$$

where $\Lambda_{nuc}(S)$ is a second nondimensional function, and L_{fric} is a length scale that will depend only on friction law parameters governing nucleation processes (in particular, it must depend on some slip or timescale in the friction law) and also on properties of the elastic medium. For linear slip-

weakening friction laws, the critical nucleation length is proportional to $\mu D_c/(\tau_p - \tau_r)$, which is remarkably independent of the initial stress level. The choice of L_{fric} is not necessarily unique. Instead, for example, the quantity $\mu D_c/(\tau_0 - \tau_r)$ could also have been chosen, which in turn introduces into Λ_{nuc} a dependence on the background loading, i.e., on S.

[18] The length scale L_{fric} enters directly from the physics of nucleation processes happening within the daughter crack and should not necessarily be identified with the length scale associated with the fracture energy at the main rupture front. It is tempting to do so, however, since this situation arises frequently in numerical modeling of ruptures under a linear slip-weakening law, or indeed, any slip-weakening law associated with a scale-independent fracture energy. Perhaps a more relevant class of friction laws is the one exhibiting continual weakening with slip, as suggested by the seismic observation of fracture energy increasing with earthquake magnitude [*Abercrombie and Rice*, 2005]. For such class of laws, the length scale governing nucleation (and for this problem, stability of the daughter crack) might be quite small, while that associated with energy dissipation processes at the main rupture front could be orders of magnitude larger. The distinction has profound implications for the extrapolation of supershear transition lengths across multiple scales, an issue which is discussed in section 7.

[19] The criterion for instability of the daughter crack, and hence the supershear transition, is simply

$$L_{dc} = L_{nuc}. \tag{3}$$

Combining equations (1), (2), and (3) yields the equation

$$L_{fric}/c_s t = \Lambda_{dc}(S)/\Lambda_{nuc}(S). \tag{4}$$

For a particular value of S, since $c_s t \propto L$, this equation has as its single unknown, the rupture length L. The value of L satisfying equation (4) defines the supershear transition length, L_{trans}, which is the distance that the main rupture must propagate before transitioning to supershear speeds.

3. Supershear Transition on Homogeneous Faults in Two Dimensions

3.1. Expanding Ruptures

[20] A convenient problem upon which to apply this analysis is that of expanding ruptures in two dimensions, the subject of the first numerical experiments to reveal supershear propagation [*Andrews*, 1976; *Das and Aki*, 1977]. The rupture properties, specifically the stress drop and friction law parameters, are spatially uniform, and the rupture expands outward from a finite nucleation zone. As *Andrews* [1976] points out, the rupture in its later stages (once it has propagated several times the extent of the finite nucleation zone) is well approximated by a self-similarly expanding crack. In the self-similar problem, stress drop and rupture speed are everywhere constant, such that the rate of stress release by the main crack is also constant. This implies that stresses and particle velocities are homogeneous of degree 0 in (x, y, t); that is, their amplitudes remain constant in time, but all associated length scales grow linearly in time. The problem also features an energy release rate at the crack tips that increases linearly in time, in contrast to the constant fracture energy condition used both by *Andrews* [1976] and in similar numerical models later in this work. As a consequence, the main discrepancy from the self-similar approximation is that ruptures in the numerical model accelerate toward the Rayleigh speed, while in the self-similar model, they expand uniformly at a constant speed. Violation of the constant rupture speed assumption will be discussed later (in section 3.3, where the self-similar model is compared to spontaneous rupture simulations).

[21] To proceed, the stress field of a self-similarly expanding rupture takes the form

$$\tau(x,t) = \tau_0 + (\tau_0 - \tau_r)\bar{\tau}(x/c_s t). \tag{5}$$

The nondimensional stress profile $\bar{\tau}(x/c_s t)$ is shown in Figure 1 (see Appendices A and B for solution details). Stress increases when the P wave arrives, reaching a maximum just prior to the S wave arrival. The S wave carries with it an inverse square-root wavefront singularity in particle acceleration and stress rate, which manifests in the rapid decrease in stress down to a minimum at the Rayleigh wave arrival. Stress then rises to a singular concentration at the rupture front. Imposing a failure criterion by setting the stress equal to the peak strength implies that at failure,

$$\bar{\tau}(x/c_s t) = (\tau_p - \tau_0)/(\tau_0 - \tau_r). \tag{6}$$

The right-hand side is the seismic S ratio. The transition cannot occur when $S > S_{max}$, and it is possible that the rupture will take the form of a single intersonic crack (rather than a sub-Rayleigh crack with a daughter crack ahead of it) when $S < S_{min}$. We again caution that using S_{min} as determined from a singular crack solution is dubious for reasons discussed before.

[22] The values of S_{max} and S_{min} depend upon the rupture process, which, in this case, are specified only by the speeds of the two crack tips. Figure 2 shows the dependence of S_{max} on these parameters. Particularly notable is the fact that S_{max} decreases rapidly with the speed of the nearest crack tip, suggesting that in order for the supershear transition to occur, either S must be quite low or the rupture speed must approach c_R. Propensity for the latter will be greatly enhanced for spontaneous ruptures once the daughter crack begins to develop: Formation of the daughter crack initiates slip and reduces the fault strength that the sub-Rayleigh main rupture encounters. Of course, in the context of the self-similar model analyzed in this section, rupture velocity is unaltered by the growth of the daughter crack.

[23] The displacement field in this model is homogeneous of degree 1, so after imposing a peak strength to generate the daughter crack, its length grows linearly in time. The length of the daughter crack, estimated as the extent of the region in the vicinity of the S wave stress peak satisfying the failure condition, is shown in Figure 3.

3.2. Self-Similar Dugdale Model

[24] The validity of these ideas can be tested by comparison of the previous predictions to numerically measured

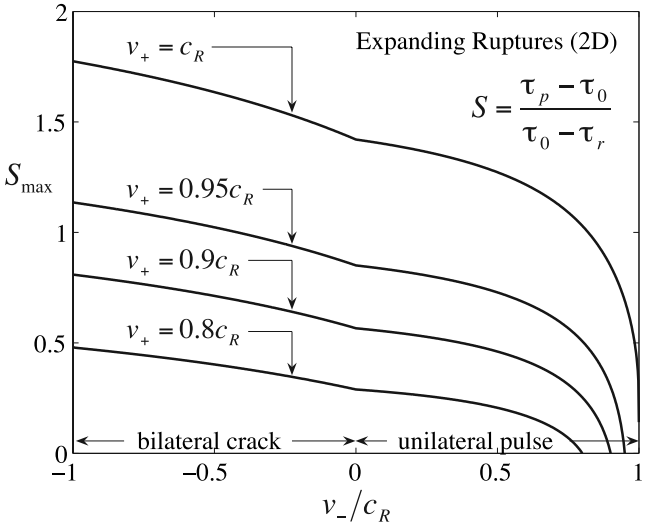

Figure 2. S_{max} for an expanding rupture, shown for various speeds of the crack tips.

transition lengths for spontaneously expanding ruptures. This requires specifying a friction law, ideally one for which the critical daughter crack length can be calculated. A suitable choice is the Dugdale model [*Dugdale*, 1960; *Barenblatt*, 1962], in which fault strength is slip-dependent and of the following form:

$$\tau_{st}(\Delta u) = \begin{cases} \tau_p \text{ for } \Delta u < d_0 \\ \tau_r \text{ for } \Delta u > d_0, \end{cases} \tag{7}$$

where Δu is the slip, and d_0 is the critical displacement.

[25] It is possible to analytically obtain an accurate estimate of the daughter crack length by enforcing the Dugdale friction law within the self-similar model. There are several regions where stresses might exceed the peak strength: at the tips of the main rupture and in the daughter crack. In the context of the Dugdale friction law, the regions over which stress equals τ_p should be interpreted as cohesive zones. When the daughter crack forms, it can be viewed as a spatially discontinuous extension of the cohesive zone beyond the tip of the main rupture, and it permits weakening to occur at intersonic speeds. If stress levels are too low for a daughter crack to form, cohesive zones appear only at the main rupture tips, and the rupture propagates at a sub-Rayleigh speed. If stress levels permit the formation of a daughter crack, it will be a passively driven extension of sub-Rayleigh main rupture's cohesive zone until the time at which the sufficient slip ($\Delta u = d_0$) occurs within the daughter crack for the entire weakening process to complete at intersonic speeds. This precise moment marks the end of the supershear transition: The intersonic daughter crack assumes the role of the primary rupture front, and the rupture propagates in a self-sustained manner at an intersonic speed.

[26] In the context of this work, it is sufficient to enforce the strength limit only within the region surrounding the *S* wave stress peak ahead of the right-moving rupture front and not within the analogous region on the other side of the opposite tip and neither at the rupture fronts themselves (it is straightforward to construct a solution that enforces these additional constraints and bounds stress everywhere on the fault, but such solution has only minor differences with the simpler solution used here at the cost of introducing additional parameters.) A particular choice of τ_p, or more precisely of *S*, uniquely defines the extent of the slipping region within a daughter crack ahead of the sub-Rayleigh rupture. The speeds of the leading and trailing edges of the daughter crack are denoted as *b* and *a*, respectively. In all cases examined, $c_R < a < c_s$ and $c_s < b < c_p$. Within the daughter crack, shear stress is equated to τ_p, under the assumption that at every point within the daughter crack, slip is less than the critical value d_0 (hence the model applies only to times prior to the supershear transition). The simplicity of this boundary condition is what renders the Dugdale friction law so desirable. Outside of the sub-Rayleigh rupture and the daughter crack, the fault is locked. Note that while the fault is locked between the trailing edge of the daughter crack and the right-moving sub-Rayleigh rupture front, slip in this region will be nonzero. Mathematically, the boundary conditions are written as

$$\begin{aligned} \sigma_{xy}(x,0,t) &= \begin{cases} \tau_r \text{ for } v_- < x/t < v_+ \\ \tau_p \text{ for } a < x/t < b \end{cases} \\ \frac{\partial u_x}{\partial t}(x,0,t) &= 0 \text{ elsewhere.} \end{aligned} \tag{8}$$

As in the previous section, v_+ and v_- are the speeds of the right and left crack tips (or of the rupture front and healing front for pulses), respectively.

[27] The solution is obtained by taking Laplace transforms over *t* and *x*, setting up and solving a Hilbert problem, and inverting the transforms with the Cagniard-de Hoop method. Solution details are given in Appendices A and B, and the main results are presented in Figure 4.

[28] The friction law (7) is enforced only within the daughter crack, while stress at the main rupture front is singular. This is likely justified for most values of *S*, especially larger ones (for which the extent of the process

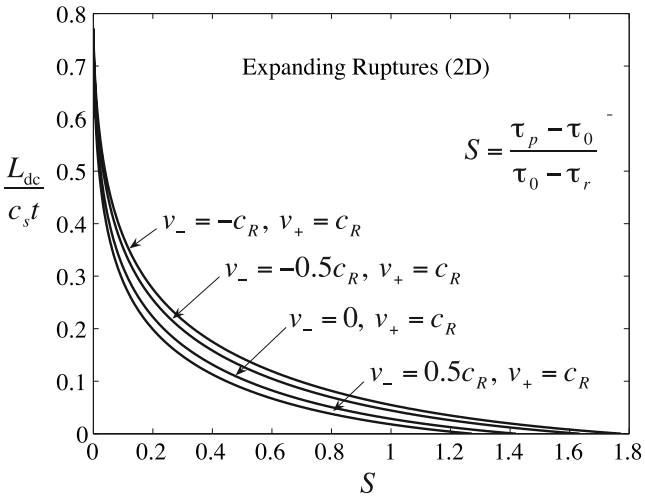

Figure 3. Estimated length of the daughter crack for expanding ruptures in two dimensions, shown for various speeds of the crack tips.

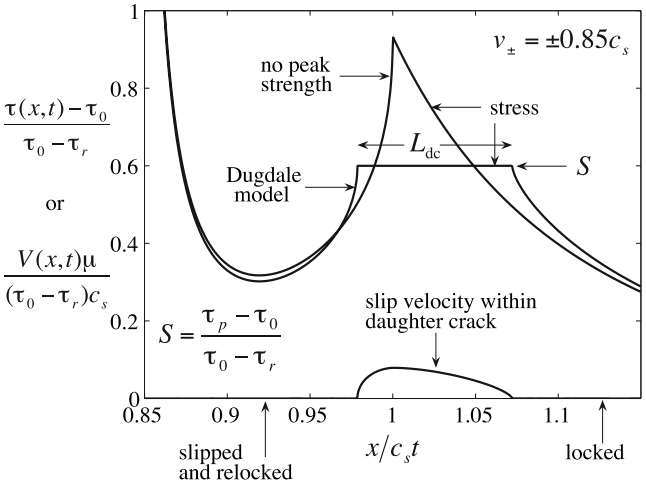

Figure 4. Solution to the self-similar Dugdale model, in which the stress field adjacent the S wave stress peak is limited to the peak strength, causing the formation of a daughter crack. Slip velocity within the daughter crack is also shown.

zone at the main rupture front diminishes). Furthermore, as the speed of the main rupture approaches the Rayleigh speed, the process zone becomes vanishingly small and the elastodynamic solution becomes quite independent of the details at the main rupture front.

[29] The self-similar model satisfies the Dugdale friction law within the daughter crack but only when slip at any point within the daughter crack remains less than d_0. The point of maximum slip occurs at the innermost edge of the daughter crack, which moves at speed a. A condition for instability can consequently be formed by combining this with an expression for slip in the self-similar solution

$$\Delta u(x,t) = \frac{\tau_0 - \tau_r}{\mu} c_s t \Delta(x/c_s t), \tag{9}$$

where $\Delta(x/c_s t)$ is a nondimensional function that depends on S and the speeds of the crack tips. Instability of the daughter crack occurs when

$$\frac{\tau_0 - \tau_r}{\mu} c_s t \Delta(a/c_s) = d_0. \tag{10}$$

[30] The frictional length scale can be taken as $L_{fric} = \mu d_0/(\tau_p - \tau_r)$ although, as mentioned previously, this choice is not unique. As the Dugdale instability condition depends upon slip reaching a specified value, and as the amplitude of slip depends on the stress drop, then the nucleation length in this model will be sensitive to the initial stress level. An alternative choice of L_{fric} that highlights the linearity of slip and stress drop is $\mu d_0/(\tau_0 - \tau_r)$; however, the previous choice will be used henceforth.

[31] The daughter crack length is $\Lambda_{dc} = (b - a)/c_s$, and the nucleation length is

$$\Lambda_{nuc}(S) = \frac{b-a}{c_s} \frac{1+S}{\Delta(a/c_s)}. \tag{11}$$

Inserting these expressions into equation (4) yields an expression for the supershear transition length:

$$\frac{L_{fric}}{L} = \frac{c_s}{v_+} \frac{\Delta(a/c_s)}{1+S}. \tag{12}$$

If instead the daughter crack length is estimated from the self-similarly expanding crack solution without an imposed peak strength, as in section 3.1 and Figure 3, then the predicted transition length will differ. Using that estimate of L_{dc} underestimates the length of the daughter crack but never by more than a factor of 2. An underestimate is to be expected since this alternative procedure neglects stress transfer between the slipping region in the daughter crack and the surrounding fault, which acts to drive further failure.

3.3. Numerical Validation

[32] The prediction (12) is compared to numerical calculations of spontaneously propagating ruptures under the Dugdale friction law in the case that d_0 and, consequently, fracture energy are constant everywhere on the fault. Rupture is nucleated by perturbing a preexisting crack in static equilibrium. The displacement field associated with this static solution, as well as details of the numerical solution, is given in Appendix C. Comparison of the analytical and numerical results is shown in Figure 5.

[33] Agreement with the predictions of the self-similar model is quite good, particularly as $S \rightarrow S_{max}$. Deviations from the predicted transition lengths are caused primarily by departure from self-similarity. The self-similar solution has the property that energy release rate grows linearly in time; this allows the rupture to expand at a constant speed. In comparison, these spontaneous ruptures grow under the condition of a constant fracture energy Γ and, consequently, must begin from a finite length and accelerate over some timescale up to the Rayleigh speed. For the case of a

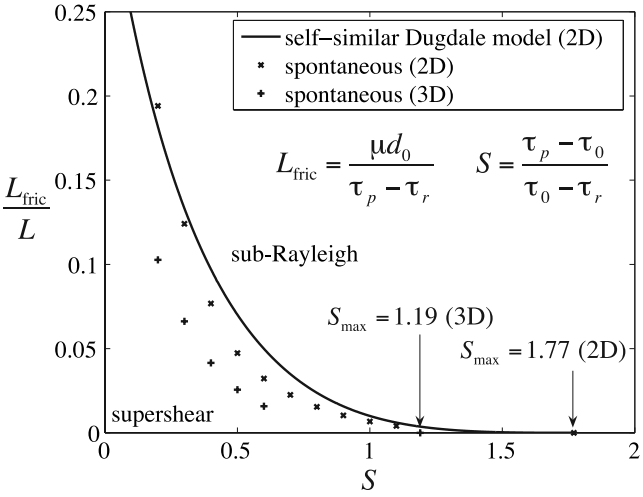

Figure 5. Supershear transition length as a function of seismic S ratio. The line marks the transition length predicted from the self-similar Dugdale model. The data points are from spontaneous rupture calculations in which the rupture is initiated by perturbing a preexisting crack in static equilibrium.

constant fracture energy, this timescale is $\sim\mu\Gamma/[(\tau_0 - \tau_r)^2 c_s]$ [*Kostrov*, 1966; *Aki and Richards*, 2002, p. 574], which translates to an acceleration distance $\sim(1 + S)^2 L_{\text{fric}}$. The numerical results in Figure 5 demonstrate that this length becomes a small fraction of the transition length as S increases.

4. Supershear Transition on Homogeneous Faults in Three Dimensions

4.1. Expanding Ruptures on Unbounded Faults

[34] Three-dimensional ruptures involve a mixture of mode-II and mode-III loading. As the supershear phenomenon is unique to mode II, it is expected to occur on portions of the rupture front experiencing predominantly mode-II conditions. The first three-dimensional rupture process considered here is that of an expanding crack on an unbounded fault with uniform stress drop and frictional parameters. This model is likely applicable to the early stages of rupture growth prior to the rupture saturating the fault width. The initial growth of a three-dimensional rupture may be approximated, then, as a self-similarly expanding elliptical crack with a constant stress drop within the slipping region of the fault. This problem has received much attention [*Burridge and Willis*, 1969; *Richards*, 1973; *Willis*, 1973; *Richards*, 1976]. As is the case in two dimensions, the stress field is homogeneous of degree 0. The results of *Richards* [1973], in particular his Figure 7, indicate the presence of a peak in shear stress in the in-plane direction ahead of a sub-Rayleigh rupture. This suggests that the supershear transition should occur by the formation of a daughter crack over some area of the fault ahead of the main rupture, at least for sufficiently small values of S. Stability of the daughter crack will depend upon its size and shape, likely in a manner similar to that found in the studies of *Favreau et al.* [2002] and *Uenishi and Rice* [2004] on quasi-static nucleation under linear slip-weakening laws in three dimensions.

[35] The self-similar elliptical crack provides a starting point for a quantitative analysis of the supershear transition in three dimensions. While *Richards* [1973] has presented a method for calculating the fields surrounding such a crack based on the Cagniard-de Hoop technique, an alternative route to the solution, given by *Willis* [1973], is taken in this work. Relevant details are summarized in Appendix D, and the results (requiring numerical integration) match the cases presented by *Richards* [1973].

[36] Calculations presented in Figure 6 confirm the existence of a stress peak moving at the S wave speed, similar to that seen for two-dimensional mode-II cracks. Its amplitude varies with position around the rupture front, attaining its maximum value in the in-plane direction. Formation of a daughter crack is expected if stresses within this region exceed the peak strength; again, the relevant nondimensional parameter is the seismic S ratio. Provided that a similar instability condition exists for the daughter crack, all of the theoretical ideas for two-dimensional ruptures will carry over directly to three dimensions.

[37] The nondimensional value of stress at the S wave stress peak, $S_{\max}$, increases with rupture speed as in two dimensions; this variation, as well as the dependence on position along the rupture front, is shown in Figure 7. The

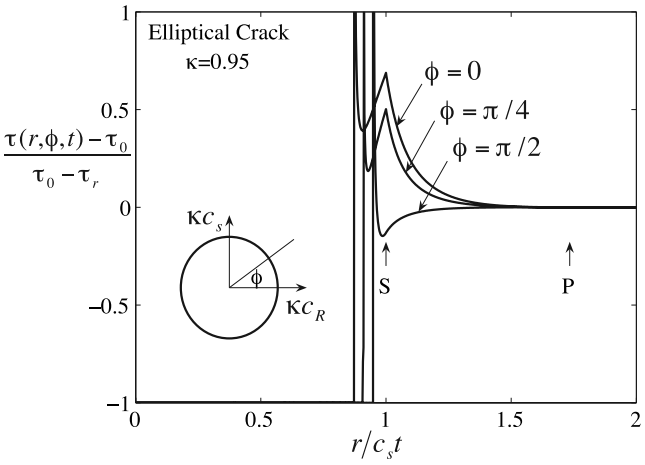

Figure 6. Stress field surrounding an expanding elliptical crack, with arrows marking the arrival of the P and S waves. The rupture velocity is κc_R in the in-plane direction and κc_s in the antiplane direction. The large value of $\kappa = 0.95$ shown here results in an extremely concentrated stress singularity at the rupture front, as well as a large S wave stress peak that is most pronounced in the in-plane ($\phi = 0$) direction.

largest value of $S_{\max}$, beyond which the supershear transition cannot occur, is 1.19 (occurring in the in-plane direction when the in-plane and antiplane rupture speeds are c_R and c_s, respectively). This is lower than the value of 1.77 for two-dimensional mode-II cracks [*Andrews*, 1985]. A lower value for the three-dimensional case is not unexpected, given that convexity of the rupture front defocuses stress-wave radiation from slip within the crack (the opposite effect, focusing by a concave rupture front, underlies the supershear transition mechanism described by *Dunham et al.* [2003]).

4.2. Expanding Ruptures on Finite-Width Faults

[38] An important extension of these ideas occurs when ruptures saturate the width of the seismogenic zone. When a rupture encounters the fault edges, arrest waves are transmitted back across the slipping region of the rupture, ultimately leading to the development of a slip pulse [*Day*, 1982a]. Once this happens, the slipping region no longer expands. As the rupture settles into steady state conditions, the S wave stress peak moves off ahead of the rupture and diminishes in amplitude due to geometrical spreading. This phenomenon can be quantified for ruptures on a fault of fixed width W in an unbounded medium. For a given transition length on an unbounded fault, denoted as $L_{\text{trans},0}$ when the context is not otherwise clear, there exists some value of W below which arrest waves arrive at the rupture front in time to inhibit the supershear transition. A rough estimate of the critical value of W can be obtained in the following manner. The daughter crack, traveling at c_s, is located at $x = L' = (c_s/v_{\text{II}})L_{\text{trans}}$ when the transition occurs, where v_{II} is the average rupture velocity along the x axis. It takes a time L'/c_s for the daughter crack to reach this point. The arrest wave must arrive at the daughter crack prior to the transition. The arrest wave is emitted from the top edge of the fault when the rupture arrives there at time $(W/2)/v_{\text{III}}$,

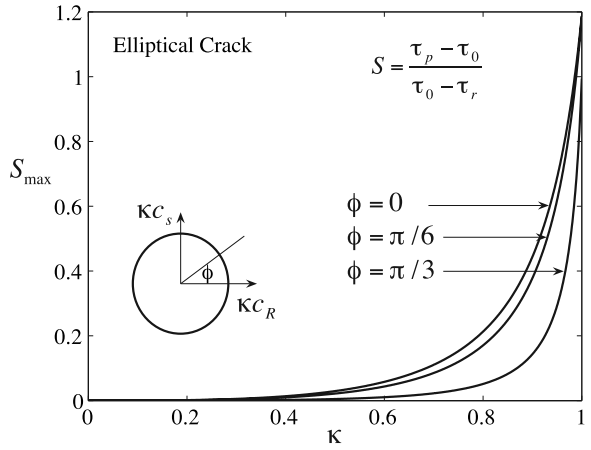

Figure 7. S_{max} for an expanding elliptical crack, shown for various speeds of the crack tips. The rupture velocity is κc_R in the in-plane direction and κc_s in the antiplane direction. The largest value of S_{max}, occurring for $\kappa = 1$ and $\phi = 0$, is 1.19.

where v_{III} is the average rupture velocity along the z axis. The arrest wave then travels a distance $\sqrt{(L')^2 + (W/2)^2}$ at speed c_a. Equating these times yields a single expression for the critical $W/L_{trans,0}$. Estimating the average rupture speeds as $v_{II} \approx c_R$ and $v_{III} \approx c_s$, and using for the arrest wave speed, the P wave speed yields $W/L_{trans,0} \approx 0.9$. Slightly decreasing the arrest wave speed decreases this estimate. Numerical modeling presented in the following section suggests a value of approximately 0.8, slightly increasing with increasing S, which is consistent with this geometrical interpretation. Dependence upon S likely arises from taking into account the decay of arrest wave amplitude due to geometrical spreading, an effect which increases with the transition length (and consequently S), but which is neglected in this simple estimate.

4.3. Numerical Validation

[39] These ideas are confirmed by numerical simulations of spontaneous rupture growth analogous to those performed in two dimensions, again using the Dugdale friction law. Ruptures are nucleated by perturbing preexisting cracks in static equilibrium. In contrast to the two-dimensional case, for which there is an analytical solution to the static problem, the three-dimensional solution must be obtained numerically. Details are given in Appendix C3. Spontaneous ruptures are first modeled on unbounded faults loaded at various levels; the resulting transition lengths are shown in Figure 5. The dynamics of the transition in three dimensions are identical to those in two dimensions in the sense that the transition length decreases monotonically with decreasing S and assumes its dimensional form in comparison to the friction length scale arising from the nucleation process of the daughter crack. The transition lengths are longer in three dimensions than in two dimensions, however, and the maximum value of S permitting the transition is lower, implying that the elliptical rupture geometry is less conducive to the transition than the straight rupture fronts in two-dimensional models.

[40] Next, a finite fault width, W, is imposed in the antiplane direction. On the basis of symmetry about the midline of the fault ($z = 0$), the resulting rupture process is quite similar to that which would occur on a vertical strike-slip fault breaking the free surface, with the depth extent of the seismogenic zone identified as $W/2$. The analogy is not strictly correct, however, as the symmetry conditions in this numerical study result in vanishing shear stress on a horizontal plane through this midline, but the desired condition of vanishing normal stress is replaced by one of the vanishing vertical displacement. The differences have not been studied in detail, but it seems unlikely that the qualitative results will differ significantly. In fact, it is well known from numerical models [*Olsen et al.*, 1997; *Aagaard et al.*, 2001; *Gonzalez*, 2003] that propensity for a supershear transition is enhanced by the free surface.

[41] Figure 8 compares the rupture history on two bounded faults to that on an unbounded fault. The values of W bound a critical width, such that as this width is approached from above, L_{trans} diverges. Ruptures on the slightly narrower fault never become intersonic, while those on the slightly wider fault do. Prior to the supershear transition, the rupture front contours are nearly identical although a slight delay in growth can be seen near the edges of the bounded faults. This difference, while minor in terms of the rupture timing, is sufficient to inhibit the growth of the daughter crack and to prevent the supershear transition.

[42] The divergence of L_{trans} actually occurs over a narrow, but finite, range of W. This is quantified from numerical results presented in Figure 9 as $W/L_{trans,0} \approx 0.8$, which increases slightly with S, at least over the limited range studied here ($0.4 \leq S \leq 0.6$). Such a result is consistent with the geometric interpretation of arrest waves arriving from the fault edges. This implies that the effective value of S_{max} for bounded faults is a decreasing function of fault width, or, in other words, that narrow faults must be loaded closer to failure than unbounded faults to permit the occurrence of supershear ruptures.

[43] The critical fault width expression may be written in an alternative form by expressing the transition length as a function of S: $L_{fric}/L_{trans} = \ell(S)$ (in which the function $\ell(S)$ is

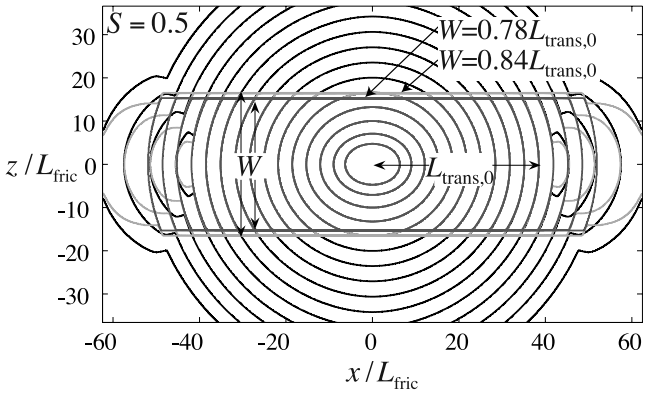

Figure 8. Rupture front contours illustrating the critical fault width ($W \approx 0.8L_{trans,0}$) for $S = 0.5$. The contours, defined as the location at which slip reaches the weakening displacement, $\Delta_u = d_0$, are plotted every 60 time steps [$=3.6585L_{fric}/c_s$] from $t = 0$ (the initial static solution). Shown are contours from ruptures on an unbounded fault (black) and on two finite-width faults (light and dark gray).

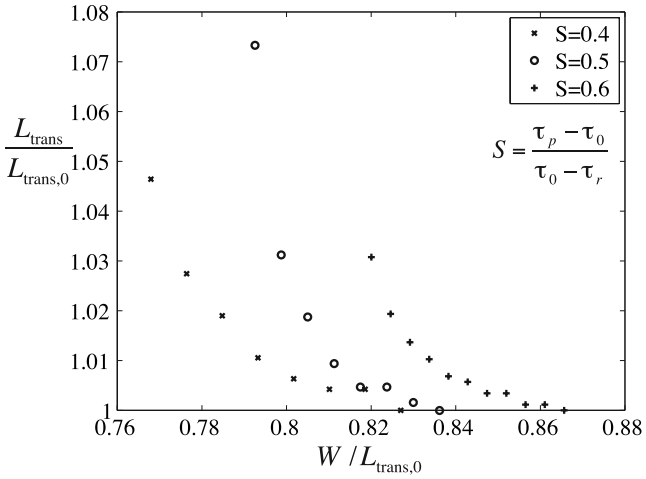

Figure 9. Divergence of the supershear transition length as the critical fault width, $W \approx 0.8L_{\text{trans},0}$, is approached, shown for several values of the seismic S ratio. The spacing in W is at the limit of the numerical spatial discretization of the fault width. The data point at the smallest value of W (for each value of S) corresponds to the narrowest fault width which still permits the supershear transition, at least at the numerical discretization level employed.

obtained from Figure 5). Noting that $W/L_{\text{fric}} = (1 + S^2)\kappa$, where $\kappa = [(\tau_0 - \tau_r)^2 W/\mu]/[(\tau_p - \tau_r)d_0]$ is the nondimensional parameter defined by *Madariaga and Olsen* [2000] and *Madariaga et al.* [2000], the condition for supershear may be written as

$$\kappa \geq 0.8(1 + S)^2/\ell(S). \tag{13}$$

This is similar to the criterion proposed by Madariaga and coworkers: that κ must exceed a critical value, κ_{cr}, to induce the transition, but has the important difference that κ_{cr} is highly dependent on S.

5. Sensitivity of Transition Length to Friction Law

[44] The supershear transition length is quite sensitive to the form of the friction law governing slip instability on the fault. This stands in contrast to the dependence of sub-Rayleigh rupture growth solely upon fracture energy due to a strong trade-off between slip-weakening distance and strength drop [*Guatteri and Spudich*, 2000]. The sensitivity of the transition length arises from a similar sensitivity of rupture nucleation processes to the form of the friction law.

[45] To explore this issue, a set of numerical experiments was conducted for two-dimensional ruptures on uniformly loaded faults. A power law slip-weakening law of the form

$$\tau_{\text{st}}(\Delta u) = \begin{cases} \tau_p - (\tau_p - \tau_r)(\Delta u/D)^p & \text{for } \Delta u < D \\ \tau_r & \text{for } \Delta u > D. \end{cases} \tag{14}$$

was used. The fracture energy for slip greater than D is $\Gamma = (\tau_p - \tau_r)Dp/(p + 1)$. To permit a comparison between different forms of the friction law, Γ is held fixed when varying p; hence the value of slip at which the residual strength is reached, D, changes with p. Spontaneous ruptures were induced for various values of p, keeping both the seismic S ratio and the fracture energy fixed. The frictional length scale is taken to be $L_{\text{fric}} = \mu d_0/(\tau_p - \tau_r)$, where d_0 is defined by $\Gamma = (\tau_p - \tau_r)d_0$. In the limit that $p \to 1$, this law becomes the Dugdale friction law used previously, and the use of d_0 here is consistent with its previous use. As before, ruptures are nucleated by perturbing preexisting static cracks (see Appendix C4 for details on the numerical procedure and static solution).

[46] Quasi-static nucleation studies under power law slip weakening (but characterized by continual weakening rather than a plateau at a well-defined τ_r) by *Rice and Uenishi* [2002] have suggested that for $p < 2/3$, instability occurs as soon as the peak strength is reached. Using such a law would raise delicate issues regarding convergence of a solution obtained numerically, and since the point of this section is not a comprehensive study of the supershear transition under power law weakening, but simply a demonstration of the sensitivity of the transition length to the form of the friction law, values of p in this range are avoided. On the other hand, rapidly weakening laws of that form might be of particular interest to the earthquake problem. *Abercrombie and Rice* [2005] suggest that seismic data, if interpreted within a slip-weakening context, are best explained by power law weakening with exponent $p \approx 0.3$. Thermal pressurization provides a theoretical framework that makes a similar prediction, but one for which the weakening rate, while initially quite large (in fact, becoming unbounded as the width of the shear zone approaches zero), eventually diminishes with increasing slip [*Rice*, 2006]. In both cases, the initial weakening rate is within the range for which instability should be immediate upon stress levels reaching the peak strength. This situation is not numerically explored here, but a discussion of possible implications appears in section 7.

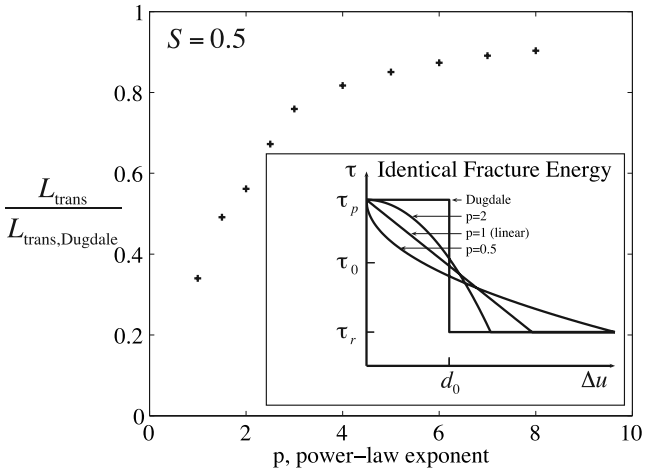

Figure 10. Supershear transition lengths under power law slip weakening with various exponents but having identical fracture energies. The Dugdale friction law emerges in the $p \to \infty$ limit, and the transition length in this limit provides the upper bound on transition lengths under slip-weakening friction laws. Inset shows power law slip-weakening constitutive law.

[47] Figure 10 shows that the transition length decreases as p decreases, in accord with the expectation that a more rapid weakening process will result in shorter nucleation lengths. In the particular case studied here ($S = 0.5$), the transition under linear slip weakening occurs in approximately a third of the distance required under the Dugdale law.

6. Supershear Transition Induced by Heterogeneous Rupture Propagation

[48] In addition to the ability of expanding ruptures to jump discontinuously from sub-Rayleigh to intersonic speeds, it is known from numerical simulations that the supershear transition can be initiated by heterogeneous rupture processes [*Fukuyama and Olsen*, 2002; *Dunham et al.*, 2003]. Ruptures accelerate in response to increases in stress drop or to decreases in fracture energy on the fault. Consider first sub-Rayleigh propagation in two dimensions; there exist important differences in the intersonic regime that will be discussed later. When ruptures accelerate, the deformation field surrounding the rupture front adapts to accommodate the new motion and possibly different energy flux into the process zone. Information regarding the change in rupture speed radiates outward from the rupture front in the form of stress waves, establishing the steady state field associated with the new propagation conditions immediately upon the slowest elastic wave arrival, rather than asymptotically in time [*Eshelby*, 1969; *Freund*, 1972b; *Kostrov*, 1975]. In the singular crack limit, this feature implies that the crack tip (idealized as a point) responds instantaneously to local variations in fracture energy. As summarized by *Freund* [1998, p. 394], an equation of motion for the crack tip can consequently be written as $G(L, \dot{L}) = \Gamma$, where $G(L, \dot{L})$ is the energy release rate of the crack as a function of its instantaneous speed, $\dot{L}$, and a functional of the history of stress release up to its current position L, and Γ is the local fracture energy (which may be spatially variable and may even be a function of rupture velocity for some materials). Prescribing a particular distribution of initial loading and fracture energy, the resulting differential equation may be integrated to obtain the crack-tip trajectory.

[49] The situation is more complicated in the intersonic regime. *Huang and Gao* [2001, 2002] and *Guo et al.* [2003b, 2003a] have extended Freund's "fundamental solution" approach to the intersonic regime, finding that the steady state dynamic stress intensity factor (the terminology is still used to describe the coefficient of the stress singularity although the singularity is weaker) is not established instantaneously as in the sub-Rayleigh regime. Consequently, the chain of reasoning leading to the sub-Rayleigh equation of motion cannot be followed. On the other hand, progress has been made in this direction. *Broberg* [1999b], using a cohesive-zone model at the crack tip, derived an expression for the stress intensity factor for accelerating intersonic cracks subject to arbitrary loading. A different approach was taken by *Obrezanova and Willis* [2003], who solved for the asymptotic structure of the crack-tip fields in the presence of small fluctuations about a steady state intersonic velocity. By combining this with the cohesive-zone model of *Antipov et al.* [2004], an approximate equation of motion is derived. A key simplifying assumption, namely, that of a small-scale cohesive zone, requires that the peak strength far exceeds the initial stress. This precludes any possibility of extending this approach to address the supershear transition. The purpose of this section is to bridge the gap left by these studies by illustrating several processes that permit jumps between the two speed regimes.

[50] The central idea here is that stress-wave radiation, induced by what would otherwise be sub-Rayleigh fluctuations of rupture speed in a singular crack model, can trigger transient supershear bursts when stresses are bound by a finite peak strength. Whether or not these transients develop into self-sustaining intersonic ruptures depends on whether or not the deformation field associated with steady intersonic propagation can become established over the duration of the supershear burst. An important caveat is in order here. The dynamics of the transition require the consideration of a process zone at crack tips, and in this work, a cohesive zone is used. The transient bursts that will be described can be thought of in the following manner: A sub-Rayleigh rupture with a cohesive zone at its tip is perturbed in such a way that a burst of stress-wave radiation causes the leading edge of the cohesive zone to surge ahead at an intersonic speed. Under certain conditions, the cohesive zone will split into two slipping regions separated by a locked region. The faster region will be propagating at an intersonic speed, while the slower part of the cohesive zone is attached to the main rupture, which will have returned now to a sub-Rayleigh speed. Instead of using a cohesive-zone model to analyze this process, singular solutions will be found that describe the stress-wave radiation induced by certain types of perturbations. The theoretical predictions must therefore be interpreted in only a qualitative sense, and a precise quantification of these predictions appears to require detailed numerical modeling.

[51] There are two main types of stress-wave radiation induced by heterogeneous rupture processes; these possess different scaling properties with regard to the time dependence of the radiated field. The first arises from variations in rupture speed in the absence of any additional stress drop, such as might arise from variations in fracture energy on the fault. The resulting radiation is transient in the sense that stress amplitudes are extremely pronounced just after jumps in rupture speed but decay as the inverse square root of time. In contrast to this, any changes in the stress drop, irrespective of whether or not the crack accelerates, generate radiation in which the amplitude of stresses remains constant in time, as was shown to be the case for expanding ruptures on homogeneous faults.

[52] The transition mechanism is readily explored in the context of a steadily propagating two-dimensional rupture which suddenly encounters some perturbation. As a starting point for a quantitative analysis, the following idealizations are made: The incident rupture is approximated as a semi-infinite mode-II crack that has been propagating for all previous time at a constant velocity v_1. Outside of the process zone, the stress field is well described by the usual singular field: $\tau(x, t) = \tau_r + K H (x - v_1 t)/\sqrt{2\pi(x - v_1 t)}$, where K is the dynamic stress intensity factor. Regularizing the stress singularity is a cohesive zone of length R. This length scale provides a lag time, R/c_s, over which the rupture responds; only for times greater than this would

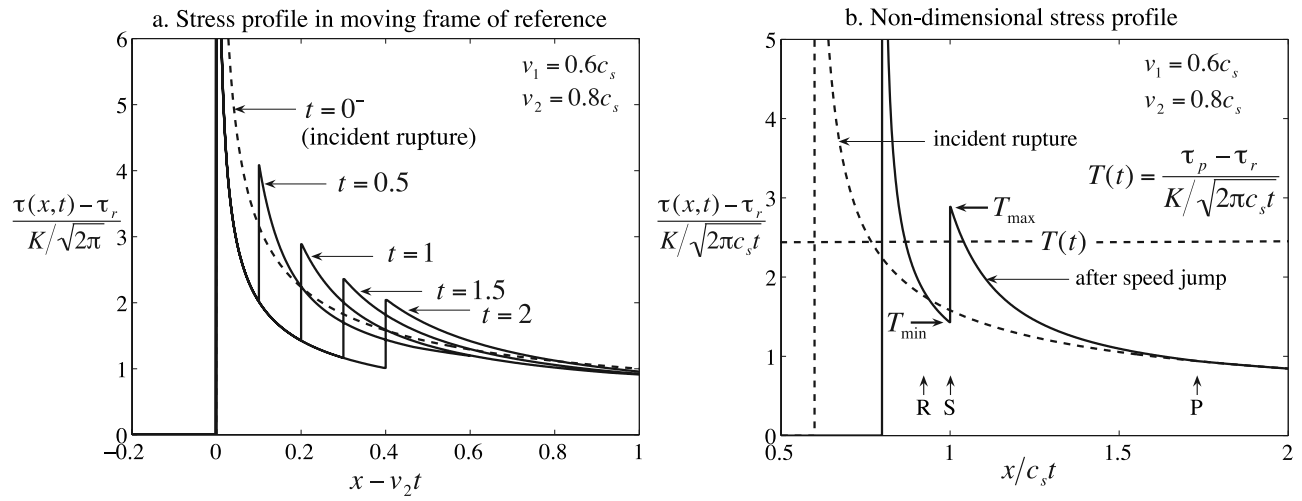

Figure 11. Stress field generated by a jump in rupture speed. Shown in Figure 11a are successive snapshots in time, illustrating the $t^{-1/2}$ decay of the stress-wave radiation. Shown in Figure 11b is the nondimensional stress field, with the nondimensional peak strength parameter $T(t)$ marked by the horizontal dashed line [note that $T(t)$ increases with time]. For (early) times such that $T(t) < T_{min}$, the "daughter crack" is merged with the main rupture front in the form of a single cohesive zone with its leading edge propagating at a supershear speed. When $T_{min} < T(t) < T_{max}$, the daughter crack emerges as a separate entity that is spatially disconnected from the main rupture. At later times such that $T > T_{max}$, the stresses associated with this transient radiation will drop below the peak strength and the intersonic daughter crack will go out of existence.

predictions based on the singular theory be valid. Approximation of the incident rupture as a steady state semi-infinite crack implies that the initial stress and residual strength are equal (i.e., $\tau_0 = \tau_r$) since no stress drop is permitted in this limit. Two types of perturbations are considered, both applied at $t = 0$ as the rupture front crosses the origin. In the first, the rupture instantaneously undergoes a step increase in speed from v_1 to $v_2 > v_1$. In the second, the stress drop increases in the region $x > 0$, parameterized here in terms of a new residual strength $\tau_r' < \tau_r$. The two effects are discussed separately in the following but, with an appropriate superposition, may act in concert.

6.1. Response to a Step Change in Rupture Speed

[53] The first type of heterogeneous rupture process considered is that of an abrupt jump in rupture speed, unaccompanied by any change in the stress drop, as might occur if a rupture encounters a region of decreased fracture energy. Numerical simulations of this situation reveal that the perturbation causes the leading edge of the cohesive zone to surge at an intersonic speed. After a short time, the cohesive zone separates into two regions, with the faster one moving at an intersonic speed and with the slower one moving at approximately the Rayleigh speed. The intersonic portion of the cohesive zone is analogous to a daughter crack that emerges from the rupture. This daughter crack eventually dies out, and the entire rupture reverts back to sub-Rayleigh propagation. The focus of this section is to explain this phenomenon.

[54] As has been pointed out [*Freund*, 1972a, 1972b; *Madariaga*, 1977], the process of crack acceleration can be viewed as the negation of the stress field of the incident rupture within the region behind the new rupture front. The total stress field for an accelerating rupture can consequently be written as the superposition of the stress field of the incident rupture and the stress field induced by a semi-infinite crack that begins at $t = 0$ and moves off at speed v_2, leaving behind its rupture front a stress drop that precisely negates the stress ahead of the incident rupture. As the rupture expands, the amplitude of the stress field to be negated diminishes as the inverse square root of distance (since the stress field of the incident rupture varies as $(x - v_1 t)^{-1/2}$). This implies that the rate of stress release decays as $t^{-1/2}$, such that the amplitude of the resulting stress-wave radiation decays with time in an identical manner (see Figure 11a). Formally stated, the stress and particle velocity fields are homogeneous of degree $-1/2$ in (x, y, t).

[55] The stress field after the speed jump, as derived in Appendices B3 and B4, takes the form

$$\tau(x,t) = \tau_r + \frac{K}{\sqrt{2\pi c_s t}}\bar{\tau}(x/c_s t). \tag{15}$$

[56] A plot of the nondimensional stress field, $\bar{\tau}(x/c_s t)$, is shown in Figure 11b. Its main features are similar to those of expanding ruptures: Stress increases from the background stress field of the incident rupture at the arrival of the P wave from the speed jump until the arrival of the S wave, where it attains its maximum value. The S wave carries with it a step discontinuity in particle velocity and stress; this feature has been extensively analyzed by *Madariaga* [1977], *Achenbach and Harris* [1978], and *Rose* [1981]. After this abrupt decrease to a local minimum, the stress field assumes the inverse square-root field associated with steady propagation at the new speed, v_2, and the correspondingly lower dynamic stress intensity factor.

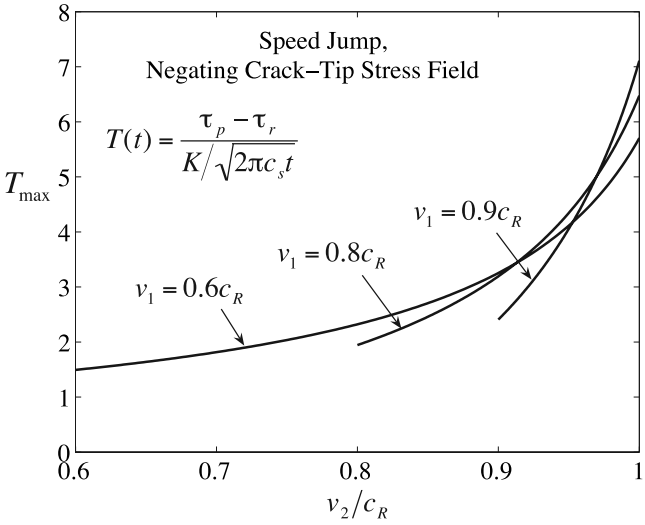

Figure 12. T_{max} for a rupture after a jump in propagation speed, shown for various speeds of the incident and accelerated rupture.

[57] Imposing a peak strength implies that at failure,

$$\bar{\tau}(x/c_s t) = \frac{(\tau_p - \tau_r)\sqrt{2\pi c_s t}}{K}. \tag{16}$$

Comparison with the analogous condition for expanding ruptures (6) shows that the dimensionless quantity on the right-hand side of equation (16), denoted hereafter as $T(t)$, plays a similar role in this problem as S does for expanding ruptures. In contrast to the expanding rupture problem where S is constant, $T(t)$ increases with the square root of time. Many of the previously developed ideas still hold: Stress levels are too low for a daughter crack to exist when $T(t) > T_{max}$, where T_{max} is the nondimensionalized value of stress at the S wave stress peak. The value of T_{max} depends on the two speeds, v_1 and v_2, as shown in Figure 12. Furthermore, the daughter crack is expected to be connected with the main rupture in the form of a single cohesive zone when $T(t) < T_{min}$, where T_{min} is the minimum value of nondimensionalized stress that occurs after the S wave discontinuity. For short times, $T(t)$ will certainly satisfy this condition.

[58] Effectively, when stresses at the rupture front are regularized by a cohesive zone, the transient radiation induced by the speed jump will cause its leading edge (but not necessarily its trailing edge) to surge forward at an intersonic speed. This situation persists until some later time, $\sim[KT_{min}/(\tau_p - \tau_r)]^2/(2\pi c_s)$, estimated from the condition $T(t) \approx T_{min}$. Around this time, the cohesive zone splits into two regions: one at a main rupture running at about the Rayleigh speed, and the second in the form of an intersonic daughter crack that has now detached from the main rupture. At a later time, given approximately by $[KT_{max}/(\tau_p - \tau_r)]^2/(2\pi c_s)$, $T(t)$ exceeds T_{max}, and the daughter crack will cease to exist. In other words, the stress-wave radiation induced by the speed jump is initially strong enough to drive the rupture front at a supershear speed but, eventually, its decaying amplitude drops below the peak strength and the rupture reverts to a sub-Rayleigh speed. This can be seen in Figure 11a.

[59] Regression back to a sub-Rayleigh speed may not always be the fate of the rupture. As numerical simulations of expanding ruptures indicate, both sub-Rayleigh and intersonic ruptures may exist under identical stress conditions for the same friction law parameters. It seems plausible that this mechanism could potentially induce a transition to self-sustained supershear propagation, provided that the stress field associated with the steady state intersonic solution could be established over a sufficiently large region surrounding the rupture, a situation which would become more likely for longer supershear bursts.

[60] The duration of the supershear transient can be roughly estimated by writing the stress intensity factor as $K = K_0 k(v_1)$, in which the static stress intensity factor may be written as $K_0 = (\tau_0 - \tau_r)\sqrt{L_K}$, and $k(v_1)$ decreases monotonically from $k(0) = 1$ to $k(c_R) = 0$ [*Fossum and Freund*, 1975]. Here $\tau_0 - \tau_r$ is the stress drop of the incident rupture, and L_K is the length scale controlling the stress intensity factor, for example, the crack length or fault width. The transient dies out when $T(t) > T_{max}$, equivalently written as

$$t > \left[\frac{k(v_1)T_{max}}{\sqrt{2\pi}(1+S)}\right]^2 \frac{L_K}{c_s}. \tag{17}$$

It is difficult to imagine that the term in brackets can ever be much larger than unity. To have an appreciable value of T_{max}, v_1 must be a significant fraction of c_R; this, however, leads to small values of $k(v_1)$, which implies that several kilometers of supershear propagation is possible for large-magnitude earthquakes.

[61] Whether or not this window of opportunity is sufficient for establishing a self-sustaining supershear rupture depends on a condition similar to that of the daughter crack reaching a critical length. In this case, it is speculated that the trailing edge of the cohesive zone must also attain an intersonic speed, which will be attained all the more readily for small values of L_{fric}. A precise quantification of this effect requires numerical modeling, but such is left for future work.

6.2. Response to a Step Change in Stress Drop

[62] If, in addition to an acceleration due to variations in fracture energy, the rupture also sustains an increased stress drop $\tau_r - \tau_r'$, the above analysis must be extended. Whether or not the additional stress drop is due to propagation into a region of increased initial stress or decreased residual strength is irrelevant at this level of approximation; both are treated identically in this singular analysis. The change in stress drop does not, in the absence of a change in fracture energy, induce an immediate change in rupture speed. Instead, the rupture responds to the history of stress release convolved with a weight function having decaying memory [*Freund*, 1998, chap. 7]. However, for the purpose of gaining insight into the radiation produced by this process, the model subsequently developed treats the rupture speed for $t > 0$ as constant. The contribution of the additional stress drop to the radiated field is that due to the appearance at $t = 0$ of a semi-infinite rupture that takes off at

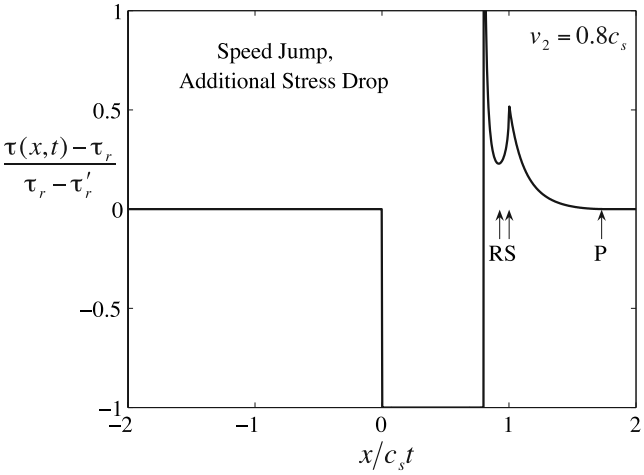

Figure 13. Additional stress field induced by an increase in stress drop, which, when added to the stress field of the incident rupture, yields the total stress field. If the rupture accelerates when it encounters the heterogeneity, the stress field of the incident rupture is replaced with the one shown in Figure 11.

speed v_2, leaving behind it over the region $0 < x < v_2 t$ an additional stress drop $\tau_r - \tau_r'$. Since this additional stress drop is spatially uniform, then the rate of additional stress release is constant in time. This implies that the stress and particle velocity fields are homogeneous of degree 0, such that the additional stress field takes the form

$$\tau(x,t) = \tau_r + (\tau_r - \tau_r')\bar{\tau}(x/c_s t), \tag{18}$$

where the nondimensional stress field, $\bar{\tau}(x/c_s t)$, is shown in Figure 13. The solution, details of which are summarized in Appendix B, is identical in its scaling properties as that associated with expanding ruptures since in both cases, the rate of stress release is constant. The nondimensional peak strength, appearing in that problem as the seismic S ratio, appears here as $S' = (\tau_p - \tau_r)/(\tau_r - \tau_r')$. This is identical to S with the stress drop in the expanding rupture problem replaced by the additional stress drop in this problem. Likewise, the maximum value of S' at the S wave stress peak can be calculated as a function of v_2, and the length of the daughter crack is estimated as was done for expanding ruptures. The results are nearly identical to those of expanding ruptures having $v_- = 0$ and $v_+ = v_2$; the only difference in boundary conditions is that the fault is locked for $x < v_- t$ in the expanding rupture problem, while it is left free to slip in this problem. The resulting differences are minor, and the reader is referred to section 3.1 for features of the stress-wave radiation (such as the variation of S_{max}' with rupture speed).

[63] The similarity of the two solutions does not mean that the supershear transition process will be identical. The major difference is that the stress-wave radiation produced by the additional stress drop must be added to the stress field of the incident rupture. While the amplitude of the radiated stress waves is constant in time, the maximum stress level moving at the S wave speed diminishes as it rides down the stress field of the incident rupture. Eventually (over a timescale determined in part by the dynamic stress intensity factor of the incident rupture), the stress level stabilizes relative to the new residual strength. Thus, while this analysis yields a value of S' that plays a similar role to the seismic S ratio, conditions for the transition are far more favorable due to the additional boost provided by the stress field of the incident rupture. Again, it is beyond the scope of this work to examine this issue in greater detail with numerical modeling; such is reserved for future efforts.

7. Discussion

[64] Ruptures jump between sub-Rayleigh and intersonic speeds when fast-moving stress waves ahead of the rupture reach the peak strength of the fault and initiate slip in the form of a daughter crack. The daughter crack may or may not be spatially connected with the main rupture according to the past rupture history and the peak strength level. Whether or not the rupture ultimately transitions to a supershear propagation velocity depends upon the stability of the daughter crack. Numerical experiments, supplemented with analytical solutions for the Dugdale friction law, confirm this reasoning. The phenomenology and scaling put forth by *Andrews* [1976] for two-dimensional ruptures carry over directly to three dimensions, at least for ruptures in uniform stress and strength conditions on unbounded faults. Interaction with a finite fault width generates arrest waves which can ultimately stifle the possibility of supershear propagation, provided that they arrive prior to the supershear transition.

[65] To summarize the main results of this study, there are two requisite conditions for sustained supershear rupture speeds to exist on a particular fault:

[66] First, the average stress level, relative to the peak and residual strengths, must be sufficiently high. If it is not, then stresses at the S wave stress peak never reach the peak strength and the daughter crack never forms (at least in the absence of any heterogeneities in the rupture process). This supershear condition is quantified in terms of the seismic S ratio as $S < S_{max}$, where small values of S indicate faults close to failure. The particular value of S_{max} depends on the rupture geometry: for two-dimensional ruptures expanding bilaterally, $S_{max} = 1.77$; for unilaterally propagating ruptures, $S_{max} = 1.42$; and for elliptical cracks, $S_{max} = 1.19$. S_{max} is further dependent on rupture speed; reducing the rupture speed from its maximum nonintersonic value (for example, c_R in the two-dimensional case) by 5 or 10% halves the value of S_{max}.

[67] Second, the daughter crack must reach a critical size and become dynamically unstable. The development of the daughter crack is determined by the rupture process and requires the rupture to have propagated some minimum distance. There are two factors which influence this distance. If the rupture process is well approximated by a self-similar solution (which occurs if stress drop is uniform and if rupture speed is constant), then stress levels ahead of the main rupture front remain constant while the length of the daughter crack increases linearly in time. The resulting transition length scales with the critical length required to nucleate ruptures. The second factor, which becomes important when ruptures depart from self-similarity, is the

distance required for a rupture to accelerate to its nonintersonic terminal velocity. The timescale of the acceleration process is determined by how the fracture energy varies with slip (and consequently with rupture length or event size). When these two factors are combined, it will be the larger of the two distances that ultimately determines the supershear transition length. In the numerical models presented in this study, a single scale-independent value of fracture energy is used. In most cases, particularly for larger values of S, the rupture accelerates to the Rayleigh speed well before the daughter crack becomes unstable. In this limit, the self-similar model does an excellent job of predicting the transition length, as evidenced by the comparison shown in Figure 5.

[68] It is unclear which factor dominates in the earth. Seismic evidence, interpreted in the context of a power law slip-weakening model (but one in which there is no well-defined residual strength, unlike the form used in this work), suggests continual weakening with slip with an exponent of about 0.3 [*Abercrombie and Rice*, 2005]. Thermal pressurization offers a similar weakening process, in particular, one that is characterized by rapid weakening at small slip [*Rice*, 2006]. Comprehensive studies of the supershear transition under such laws are certainly needed. An additional need at this point is an understanding of how the stress field develops ahead of an actual rupture as it grows across multiple scales, which requires knowledge of how fracture energy and stress drop evolve as the rupture grows.

[69] A further result of this study is that the specific form of the slip-weakening friction law exerts a large influence on the resulting supershear transition lengths. It is consequently a major concern as to whether such spontaneous rupture models, as currently implemented, can be used to determine the propensity for ruptures to become supershear even if stress conditions are accurately known.

[70] Even if the conditions summarized above are not satisfied on a particular fault, supershear propagation, at least in the form of transient bursts, remains a possibility. When ruptures encounter heterogeneities, stress waves are produced. If these waves have sufficient amplitude, they can trigger short-lived periods of supershear propagation. It remains an open question as to whether or not the duration of these transients is sufficient to cause a permanent switch in rupture speed.

Appendix A: Cagniard Inversion Formula

[71] The Cagniard-de Hoop method is used extensively in this work to invert Laplace-domain solutions of self-similar rupture problems. Description of the method can be found in numerous places, for example, in the works of *Broberg* [1999a, pp. 339–401], *Aki and Richards* [2002, pp. 218–235], and *Pao and Gajewski* [1977].

[72] A field $f(x, y, t)$ that is homogeneous of degree n is considered, such that $f(x, y, t) = t^n f_0(x/t, y/t)$. For mode II, any field can be split into dilatational and shear contributions as $f(x, y, t) = f^p(x, y, t) + f^s(x, y, t)$. Expressions will be obtained using double Laplace transforms, defined as

$$F(\zeta) = s^{n+2} \int_{-\infty}^{\infty} e^{-s\zeta x} \int_0^{\infty} e^{-st} f(x, 0, t) dt dx. \qquad \text{(A1)}$$

Table A1. Dilatational and Shear Contributions to the Displacement and Stress Fields in the Transform Domain in Terms of Either $\Sigma(\zeta)$ or $U(\zeta)$[a]

Field, $F(\zeta)$	P Contribution, $F^p(\zeta)$	S contribution, $F^s(\zeta)$
$U_x(\zeta)$	$\zeta A^p(\zeta)$	$-\beta(\zeta)A^s(\zeta)$
$U_y(\zeta)$	$-\alpha(\zeta)A^p(\zeta)$	$-\zeta A^s(\zeta)$
$\Sigma_{xx}(\zeta)$	$\mu[\zeta^2 + \beta^2(\zeta) - 2\alpha^2(\zeta)]A^p(\zeta)$	$-2\mu\zeta\beta(\zeta)A^s(\zeta)$
$\Sigma_{xy}(\zeta)$	$-2\mu\zeta\alpha(\zeta)A^p(\zeta)$	$\mu[\beta^2(\zeta) - \zeta^2]A^s(\zeta)$
$\Sigma_{yy}(\zeta)$	$\mu[\beta^2(\zeta) - \zeta^2]A^p(\zeta)$	$2\mu\zeta\beta(\zeta)A^s(\zeta)$

[a] If $\Sigma(\zeta)$ is known, then $A^p(\zeta) = -2\,\zeta\beta(\zeta)\Sigma(\zeta)/\mu R(\zeta)$ and $A^s(\zeta) = [\beta^2(\zeta) - \zeta^2]\Sigma(\zeta)/\mu R(\zeta)$. If $U(\zeta)$ is known, then $A^p(\zeta) = 2c_s^{-2}\zeta U(\zeta)$ and $A^s(\zeta) = -c_s^{-2}[\beta^2(\zeta) - \zeta^2]U(\zeta)/\beta(\zeta)$.

In general, ζ is complex, and the transforms of the dilatational and shear contributions are denoted as $F^p(\zeta)$ and $F^s(\zeta)$. Transforms of stresses and displacements are designated as $\Sigma_{ij}(\zeta)$ and $U_i(\zeta)$, respectively. For mode-II symmetry conditions, boundary conditions are given in terms of $\sigma_{xy}(x, 0, t)$ and $u_x(x, 0^+, t)$ (or their time derivatives); the transforms of these fields are designated as $\Sigma(\zeta) = \Sigma_{xy}(\zeta)$ and $U(\zeta) = U_x(\zeta)$.

[73] The Cagniard inversion formula provides an expression for $f(x, y, t)$ in terms of its transform:

$$\begin{aligned} f(x,y,t) &= \frac{1}{\pi\Gamma(n+1)}\mathrm{Im}\int_0^t \left\{F^p\left[\zeta_p(t')\right]\frac{d\zeta_p(t')}{dt'} \right. \\ &\quad \left. + F^s[\zeta_s(t')]\frac{d\zeta_s(t')}{dt'}\right\}(t-t')^n dt', \quad \text{for } n \neq -1 \\ f(x,y,t) &= \frac{1}{\pi}\mathrm{Im}\left\{F^p\left[\zeta_p(t)\right]\frac{d\zeta_p(t)}{dt}\right. \\ &\quad \left. + F^s[\zeta_s(t)]\frac{d\zeta_s(t)}{dt}\right\}, \text{for } n = -1, \end{aligned} \qquad \text{(A2)}$$

where $\Gamma(\cdot)$ is the gamma function and

$$\zeta_w(t) = \begin{cases} \dfrac{-tx + \mathrm{sgn}(x)|y|\sqrt{r^2/c_w^2 - t^2}}{r^2} & \text{for } t < r/c_w \\ \dfrac{-tx + i|y|\sqrt{t^2 - r^2/c_w^2}}{r^2} & \text{for } t > r/c_w, \end{cases} \qquad \text{(A3)}$$

such that

$$\frac{d\zeta_w}{dt}(t) = \begin{cases} -\dfrac{x}{r^2} - \dfrac{\mathrm{sgn}(x)|y|t}{r^2\sqrt{r^2/c_w^2 - t^2}} & \text{for } t < r/c_w \\ -\dfrac{x}{r^2} + i\dfrac{|y|t}{r^2\sqrt{t^2 - r^2/c_w^2}} & \text{for } t > r/c_w. \end{cases} \qquad \text{(A4)}$$

In these expressions, $r = \sqrt{x^2 + y^2}$ and the wave contributions are designated by $w = p$ or s. The terms $U_i^w(\zeta)$ and $\Sigma_{ij}^w(\zeta)$ are the dilatational and shear contributions to the displacement and stress fields, respectively, and can be written in terms of either $U(\zeta)$ or $\Sigma(\zeta)$, depending on how the boundary conditions are specified (see Table A1).

[74] The integral in equation (A2) is simply the sum of the integrals of the two wave contributions, $\mathrm{Im}[F^w(z)]$, taken along the Cagniard path $z = \zeta_w(t')$ defined by equation (A3) and parameterized by the real variable t', such that $dz = (d\zeta_w/dt')dt'$. This parameterization has the advantage of a physical interpretation in which t' is the elapsed time at the

observation point (x, y) and the integral represents the cumulative response, integrated over time, of the medium at that point to the incoming dilatational and shear waves. However, it is poorly suited for numerical evaluation. Instead, it is advantageous to deform the integration path away from the Cagniard path, which is permitted by the analyticity of the integrand so long as the path deformation does not cross any branch cuts or poles and the new path begins at some point on the real axis between the branch points and terminates at the Cagniard point $\zeta_w(t)$. Such a deformation eliminates inverse square-root singularities at the branch points, i.e., when $t' = r/c_w$. These singularities appear in $d\zeta_w/dt'$ [see equation (A4)] and correspond to singularities of the same order in $\partial^{n+1} f(x, y, t)/\partial t^{n+1}$ at the wavefronts. The path deformation further avoids the strong singular or near-singular behavior of the integrand at or near the Rayleigh poles at $\pm 1/c_R$. In practice, a semicircular contour extending from the origin to $\zeta_w(t)$ is an easily parameterized replacement to the Cagniard path.

[75] For the special case that $n = -1$ and $y = 0$, equation (A2) may be written as

$$f(x,0,t) = -\frac{1}{2\pi i x}\left[F^+(\xi) - F^-(\xi)\right]_{\xi=-t/x} \tag{A5}$$

The superscripts + and − denote the limiting value of a function in the complex plane as the real axis is approached from above or below. The imaginary part in equation (A2) has been expressed in terms of the jump of $F(\zeta)$ across the real axis. This form is particularly useful when setting up Hilbert problems as discussed in Appendix B.

Appendix B: Construction of Crack Solutions: Hilbert Problem Formulation

[76] A variety of two-dimensional self-similar crack and pulse solutions are used in this work; this appendix gives details of the construction of these solutions; a few have appeared previously in the literature, while others are newly derived here. For several problems, there are a number of alternative solution methods; this appendix uses the Hilbert problem formulation. The approach is standard for elasticity problems and is discussed by *Muskhelishvili* [1953, pp. 230–238] in the static elasticity context.

[77] The problems treated here are mixed boundary value problems, in which stress is given over some portion of the fault, and displacement (or some time derivative of these fields) is specified on the remainder. The solutions will be constructed in the transform domain, with the Cagniard inversion formula (A2) providing a link between the physical and transform domains.

B1. Expanding Cracks and Pulses

[78] To begin, consider the class of problems in which stress and particle velocity are homogeneous of degree 0, which includes bilaterally expanding cracks and unilaterally expanding pulses with a constant stress drop. The speeds of the two rupture tips are $v_\pm$, with positive speeds denoting motion in the $+x$ direction. In this case, the problem is most efficiently formulated in terms of stress rate and particle acceleration. These fields are homogeneous of degree -1, and their values on the fault may be written using equation (A5) as

$$\begin{aligned}\frac{\partial^2 u_x}{\partial t^2}(x,0^+,t) &= -\frac{1}{2\pi i x}\left[U^+(\xi) - U^-(\xi)\right]_{\xi=-t/x}\\ \frac{\partial \sigma_{xy}}{\partial t}(x,0,t) &= -\frac{1}{2\pi i x}\left[\Sigma^+(\xi) - \Sigma^-(\xi)\right]_{\xi=-t/x},\end{aligned} \tag{B1}$$

where, as stated before, the + and − signs denote the limiting value of a function as the real axis is approached from above or below.

[79] Elasticity and the assumption of mode-II symmetry conditions provide a relation between the transforms of stress and displacement:

$$\Sigma(\zeta) = -\mu B(\zeta) U(\zeta), \quad \text{with} \quad B(\zeta) = c_s^2 R(\zeta)/\beta(\zeta). \tag{B2}$$

In these expressions,

$$\begin{aligned}\alpha(\zeta) &= \sqrt{1/c_p^2 - \zeta^2}\\ \beta(\zeta) &= \sqrt{1/c_s^2 - \zeta^2}\\ R(\zeta) &= 4\zeta^2\alpha(\zeta)\beta(\zeta) + \left[\beta^2(\zeta) - \zeta^2\right]^2.\end{aligned} \tag{B3}$$

Branch cuts for $\alpha(\zeta)$ extend from branch points at $\zeta = \pm 1/c_p$ to $\pm\infty$ and likewise for $\beta(\zeta)$, with the branch chosen to ensure $\mathrm{Re}[\alpha(\zeta)] \geq 0$ and $\mathrm{Re}[\beta(\zeta)] \geq 0$.

[80] The boundary conditions in the transform domain, obtained by replacing known values in the left-hand side of equation (B1), take the general form

$$\Sigma^+(\xi) - \Sigma^-(\xi) = \Sigma_0(\xi) \tag{B4}$$

over segments of specified stress, and

$$U^+(\xi) - U^-(\xi) = U_0(\xi) \tag{B5}$$

over segments of specified displacement, where $\Sigma_0(\xi)$ and $U_0(\xi)$ are the transforms of the stresses and displacements, respectively, given as boundary conditions. The transform-domain expressions are written in terms of $\xi = -t/x$, implying the physical interpretation of $-\xi^{-1}$ as the phase velocity of the solution along the fault. The left half of the complex ζ plane corresponds to waves moving in the positive x direction and vice versa.

[81] At this point, either $\Sigma(\zeta)$ or $U(\zeta)$ may be sought; once one is obtained, the other is available from equation (B2). The choice is arbitrary, but often one leads to simpler expressions in the end. To provide a concrete example, the remainder of this discussion will focus on the problem of an expanding rupture with a daughter crack on one side (the problem considered in section 3.2). A constant stress drop is applied within the main rupture. Stresses within the daughter crack are relaxed to the peak strength, τ_p, by allowing slip over the region surrounding the S wave stress peak. The boundary conditions are given by equation (8), implying that the source terms $\Sigma_0(\xi)$ and $U_0(\xi)$ appearing in equations (B4) and (B5) are both zero (which is not to say that the stress is zero inside either the main or daughter crack; since the problem is formulated in terms of stress rate, it is this quantity which

vanishes inside the slipping portions of the fault). Furthermore, the following results are given first for nonzero $U_0(\xi)$ and $\Sigma_0(\xi)$, as these functions will be nonzero in several problems considered later.

[82] To solve for $U(\zeta)$, the next step is to convert the stress boundary condition into one on displacement by rewriting equation (B4) using equation (B2) as

$$U^+(\xi) - \frac{B^-(\xi)}{B^+(\xi)} U^-(\xi) = -\frac{\Sigma_0(\xi)}{\mu B^+(\xi)}, \tag{B6}$$

which holds over segments of specified stress. For the bilaterally expanding crack problem, these segments are $-\infty < \xi < -1/v_+$, $-1/a < \xi < -1/b$, and $-1/v_- < \xi < \infty$, while for the unilaterally expanding pulse problem, these are $-1/v_- < \xi < -1/v_+$ and $-1/a < \xi < -1/b$.

[83] The objective now is to combine equations (B5) and (B6), each of which holds on its respective segments of the real axis, into a single expression that holds for all ξ of the form

$$\frac{U^+(\xi)}{X^+(\xi)} - \frac{U^-(\xi)}{X^-(\xi)} = \frac{F_0(\xi)}{X^+(\xi)}, \tag{B7}$$

where the factor $X^+(\xi)$ on the right-hand side is inserted for later convenience. The function $X(\zeta)$ is analytic, except perhaps on the real axis, and represents the solution to the homogeneous form of equation (B7) (i.e., that which is obtained by setting $F_0(\xi) = 0$). If ξ lies within the region where stress boundary conditions are given, then comparison with equation (B6) reveals that $X^+(\xi)/X^-(\xi) = B^-(\xi)/B^+(\xi)$ and $F_0(\xi) = -\Sigma_0(\xi)/[\mu B^+(\xi)]$. If ξ lies within the region where displacement boundary conditions are given, then equation (B7) is satisfied if $X^+(\xi)/X^-(\xi) = 1$ and $F_0(\xi) = U_0(\xi)$. It is thus evident that $F_0(\xi)$ represents the inhomogeneous terms $U_0(\xi)$ and $\Sigma_0(\xi)$, expressed in terms of transformed displacements.

[84] The homogeneous solution $X(\zeta)$ is determined by the deformation mode, due to the dependence upon $B(\zeta)$, and the locations of regions where stress and displacement are specified. It is constructed by exploiting the fact that $X(\zeta)$, and hence $\ln X(\zeta)$, is analytic in the complex plane, except across branch cuts on the real axis, and that the jump in $\ln X(\zeta)$ across these cuts, alternatively written as $\ln X^+(\xi) - \ln X^-(\xi) = \ln [X^+(\xi)/X^-(\xi)]$ is known from the arguments detailed in the previous paragraph. The Cauchy integral formula can then be used to express the value of $\ln X(\zeta)$ at some arbitrary point ζ in terms of the known values of $\ln X(\zeta)$ along the line segment. This is a standard technique in complex-variable formulations of elasticity problems; for related discussion, see the works of *Broberg* [1999a, pp. 419–420] and *Muskhelishvili* [1953, pp. 230–234].

[85] Before carrying this out, note that

$$\frac{B^+(\xi)}{B^-(\xi)} = \begin{cases} 1 & \text{for} |\xi| < 1/c_p \\ -1 & \text{for } |\xi| > 1/c_s \\ e^{-2\pi i q(\xi)} & \text{for } 1/c_p < \xi < 1/c_s \\ e^{2\pi i q(\xi)} & \text{for } -1/c_s < \xi < -1/c_p, \end{cases} \tag{B8}$$

where

$$q(\xi) = \frac{1}{\pi} \arctan \frac{4\xi^2 |\alpha(\xi)||\beta(\xi)|}{\left(1/c_s^2 - 2\xi^2\right)^2}. \tag{B9}$$

To compactly represent later results, it is useful to define

$$S(\zeta; v_1, v_2) = \exp\left[\int_{-1/v_1}^{-1/v_2} \frac{q(\xi)}{\xi - \zeta} d\xi\right] = \exp\left[-\int_{1/v_2}^{1/v_1} \frac{q(\xi)}{\xi + \zeta} d\xi\right], \tag{B10}$$

with $q(\xi)$ given in equation (B9) and subject to the constraint $c_s \le v_1 < v_2 \le c_p$. This function is analytic except for a branch cut between $-1/v_1$ and $-1/v_2$, across which it satisfies

$$S^+(\xi; v_1, v_2)/S^-(\xi; v_1, v_2) = e^{2\pi i q(\xi)}. \tag{B11}$$

Furthermore, $S(\zeta; v_1, v_2) \to 1$, as $|\zeta| \to \infty$, and has the asymptotic behavior

$$\begin{array}{ll} S(\zeta; v_1, v_2) \sim (\zeta + 1/v_1)^{-q(1/v_1)} & \text{as } \zeta \to -1/v_1 \\ S(\zeta; v_1, v_2) \sim (\zeta + 1/v_2)^{q(1/v_2)} & \text{as } \zeta \to -1/v_2. \end{array} \tag{B12}$$

Note also that $S(-\zeta; v_1, v_2)$ has a branch cut between $1/v_2$ and $1/v_1$, across which

$$S^+(-\xi; v_1, v_2)/S^-(-\xi; v_1, v_2) = e^{-2\pi i q(\xi)}. \tag{B13}$$

It further has the asymptotic behavior

$$\begin{array}{ll} S(-\zeta; v_1, v_2) \sim (\zeta - 1/v_1)^{-q(1/v_1)} & \text{as } \zeta \to 1/v_1 \\ S(-\zeta; v_1, v_2) \sim (\zeta - 1/v_2)^{q(1/v_2)} & \text{as } \zeta \to 1/v_2. \end{array} \tag{B14}$$

This definition conforms to the usual definition of the function $S_\pm(\zeta)$, arising in the Weiner-Hopf factorization of the Rayleigh function, equivalent in our notation to $S(\pm\zeta; c_s, c_p)$, as in the work of *Freund* [1998, p. 88], *Kostrov* [1975], *Broberg* [1999a, p.441], etc. In a work on accelerating intersonic cracks, *Broberg* [1999b] defines a related function, which he also denotes $S(\zeta)$, that is the reciprocal of the function defined here, but when solving another problem using the Hilbert problem formulation, *Broberg* [1999a, pp. 452–454] defines the function as it is defined here.

[86] $X(\zeta)$ is then determined by evaluating the contour integral

$$\ln X(\zeta) = \frac{1}{2\pi i} \int \frac{\ln X(z)}{z - \zeta} dz. \tag{B15}$$

The particular contour of integration in this case consists of a counterclockwise circle at infinity, the contribution of which vanishes, and clockwise contours encircling the portions of the real axis on which stress boundary conditions are given (in the regions where displacement is given, $\ln X(\zeta)$ is continuous across the real axis). Evaluating the integral, and using the simplifying notation (B10), yields for $v_- < 0$

$$X(\zeta) = \frac{\sqrt{\zeta + 1/c_s}}{S(\zeta; c_s, b)(\zeta + 1/v_+)^{3/2}(\zeta + 1/v_-)^{3/2}\sqrt{\zeta + 1/a}}. \tag{B16}$$

The multivalued nature of the complex logarithm permits some flexibility in the exponents that appear; alternative solutions may add some integer to the exponent (with some restrictions; see the work of *Muskhelishvili* [1953, pp. 228, 230–232] for a precise discussion). This point has also been made by *Nielsen and Madariaga* [2003] in their study of expanding rupture pulses. The particular choices made here ensure bounded strain energy and the desired asymptotic behavior at the crack tips and the ends of the daughter crack. In particular, stress at the crack tips is square-root singular, while stress at the ends of the daughter crack is bounded.

[87] A similar analysis for the unilaterally expanding pulse (i.e., $v_- > 0$), this time requiring that stresses at the healing edge of the sub-Rayleigh rupture be nonsingular (corresponding to energy-neutral healing), yields

$$X(\zeta) = \frac{\sqrt{\zeta + 1/c_s}}{S(\zeta; c_s, b)(\zeta + 1/v_+)^{3/2}\sqrt{\zeta + 1/v_-}\sqrt{\zeta + 1/a}}. \quad \text{(B17)}$$

Now that $X(\zeta)$ has been determined; equation (B7) is solved using a second application of the Cauchy integral formula to yield

$$\frac{U(\zeta)}{X(\zeta)} = \frac{1}{2\pi i}\int_{-\infty}^{\infty} \frac{F_0(\xi)}{X^+(\xi)}\frac{d\xi}{\xi - \zeta} + P(\zeta), \quad \text{(B18)}$$

where $P(\zeta)$ is a polynomial, which permits the addition of homogeneous solutions to the particular solution given by the first term on the right-hand side of equation (B18).

[88] There are no sources for the problem at hand, so the integral term vanishes, leaving only the homogeneous solution $U(\zeta) = P(\zeta)X(\zeta)$. The polynomial $P(\zeta)$ reduces to a constant, P_0, whose value must be determined by additional constraints discussed below.

[89] The solutions, equations (B16) and (B17), for arbitrary a, b, and P_0 satisfy the boundary conditions that the stress rate vanishes within the main and daughter crack and that the slip acceleration vanishes elsewhere. However, the desired solution specifies particular values of stress within the main rupture and within the daughter crack and an exactly vanishing slip velocity between the two slipping regions. To do so requires enforcing three additional equations:

$$\begin{aligned} \frac{\sigma_{xy}(x,0,t) - \tau_0}{\tau_0 - \tau_r} &= -1 \quad \text{for } v_- < x/t < v_+ \\ \frac{\sigma_{xy}(x,0,t) - \tau_0}{\tau_0 - \tau_r} &= S \quad \text{for } a < x/t < b \\ \frac{\partial u_x}{\partial t}(x,0^+,t) &= 0 \quad \text{for } v_+ < x/t < a \end{aligned} \quad \text{(B19)}$$

[90] The expressions on the left-hand side are readily evaluated using the Cagniard inversion formula, and a nonlinear equation solver (for example, Newton's method) can be used to determine a, b, and P_0.

[91] The homogeneous solutions for the Dugdale model, equations (B16) and (B17), are easily modified if slip is not allowed within the daughter crack. In this case, $X(\zeta)$ must be continuous over the region $-1/a < \xi < -1/b$. Repeating the derivation with this constraint yields $X(\zeta) = (\zeta + 1/v_+)^{-3/2}(\zeta + 1/v_-)^{-3/2}$ for expanding cracks and $X(\zeta) = (\zeta + 1/v_+)^{-3/2}(\zeta + 1/v_-)^{-1/2}$ for expanding pulses. The crack solution matches the one given by *Burridge* [1973], which is summarized by both *Freund* [1998, pp. 330–335] and *Broberg* [1999a, pp. 414–418]. The pulse solution matches that found by S. Nielsen (personal communication, 2005) as an extension of the mode-III pulse solution by *Nielsen and Madariaga* [2003]. *Broberg* [1999a, p. 418] has also shown how such a solution arises from the general crack solution in the limit that both crack tips propagate in the same direction and the stress intensity factor at the trailing edge of the pulse is required to vanish (corresponding to the condition of energy-neutral healing).

B2. Semi-infinite Cracks With Trailing Loads

[92] A second application of the Hilbert problem method is to solve the following problem: A semi-infinite crack appears at $t = 0$ and extends from the origin at speed v_2, leaving behind it a load of constant magnitude $\tau_r - \tau_r'$, the trailing edge of which remains at the origin. This problem is homogeneous of degree 0 in stress and particle velocity. Formulation as a Hilbert problem proceeds as before except that it is easier to seek a solution for $\Sigma(\zeta)$ instead of $U(\zeta)$.

[93] In this case, equation (B7) is replaced by

$$\frac{\Sigma^+(\xi)}{Y^+(\xi)} - \frac{\Sigma^-(\xi)}{Y^-(\xi)} = \frac{G_0(\xi)}{Y^+(\xi)} \quad \text{for all } \xi, \quad \text{(B20)}$$

where $Y(\zeta)$ is the homogeneous solution for the transform of stress. This equation results from the combination of equations (B4) and (B5), with the displacement boundary condition (B5) converted to one on stress as

$$\Sigma^+(\xi) - \frac{B^+(\xi)}{B^-(\xi)}\Sigma^-(\xi) = -\mu B^+(\xi)U_0(\xi). \quad \text{(B21)}$$

In the displacement-specified region, where equation (B21) holds, $Y^+(\xi)/Y^-(\xi) = B^+(\xi)/B^-(\xi)$ and $G_0(\xi) = -\mu B^+(\xi)U_0(\xi)$, while in the stress-specified region, $Y^+(\xi)/Y^-(\xi) = 1$ and $G_0(\xi) = \Sigma_0(\zeta)$. The solution to equation (B20), obtained as before, is

$$\frac{\Sigma(\zeta)}{Y(\zeta)} = \frac{1}{2\pi i}\int_{-\infty}^{\infty} \frac{G_0(\xi)}{Y^+(\xi)}\frac{d\xi}{\xi - \zeta} + P(\zeta), \quad \text{(B22)}$$

where $P(\zeta)$ is again a polynomial.

[94] Applied to the problem at hand, the homogeneous solution is found to be

$$Y(\zeta) = \frac{S(\zeta; c_s, c_p)(\zeta + 1/c_R)}{(\zeta + 1/v_2)^{3/2}\sqrt{\zeta + 1/c_s}}, \quad \text{(B23)}$$

where $S(\zeta; c_s, c_p)$ is given in equation (B10). The transform of the load is given by

$$\Sigma_0(\xi) = 2\pi i(\tau_r - \tau_r')\delta(\xi). \quad \text{(B24)}$$

[95] In contrast to the previously treated problem, the solution of interest is now the particular solution, obtained by evaluating the integral in equation (B22) to account for nonzero stress rates within the slipping portion of the fault

(the delta function in the above equation). The solution is consequently

$$\Sigma(\zeta) = \frac{(\tau_r - \tau_r')Y(\zeta)}{\zeta Y(0)}. \quad \text{(B25)}$$

This result matches the solution given by *Broberg* [1999a, pp. 439–449], who also allows for the trailing edge of the load to move at an arbitrary speed.

B3. Jump in Rupture Speed

[96] A further application of the Hilbert problem method is to the case of a semi-infinite crack, initially propagating under steady state conditions at speed v_1, that instantaneously accelerates at $t = 0$ to speed $v_2 > v_1$. The total field induced by this rupture can be written as the superposition of that from the original steady state rupture, and the field induced by a semi-infinite crack that appears at $t = 0$ with its tip at the origin, which, as it propagates away at v_2, negates the stress field of the incident rupture:

$$\sigma_0(x,t) = -\frac{KH(x - v_1 t)}{\sqrt{2\pi(x - v_1 t)}}. \quad \text{(B26)}$$

[97] A few differences from the previously treated problems appear in this case, however, since stresses and particle velocities are homogeneous of degree $-1/2$. The Cagniard inversion formula (A2), when applied to shear stress on the fault, reads

$$\sigma_{xy}(x,0,t) = -\frac{1}{2\pi^{3/2} i x}\frac{1}{\sqrt{t}} * [\Sigma^+(\xi) - \Sigma^-(\xi)]_{\xi=-t/x}, \quad \text{(B27)}$$

where * denotes convolution over time.

[98] The load is simply the transform of equation (B26):

$$\Sigma_0(\xi) = -\frac{K}{\sqrt{2\xi}(1 + v_1\xi)}. \quad \text{(B28)}$$

A Hilbert problem is then formulated as in equations (B4) and (B5), with nonzero $\Sigma_0(\xi)$ given by equation (B28). The problem becomes

$$\Sigma^+(\xi) - \Sigma^-(\xi) = \begin{cases} 0 & \text{for } -\infty < \xi < -1/v_1 \\ \Sigma_0(\xi) & \text{for } -1/v_1 < \xi < -1/v_2 \\ 0 & \text{for } 1/c_p < \xi < \infty \end{cases} \quad \text{(B29)}$$

$$U^+(\xi) - U^-(\xi) = 0 \quad \text{for } -1/v_2 < \xi < -1/c_p. \quad \text{(B30)}$$

In this case, it is easier to solve for $\Sigma(\zeta)$ than $U(\zeta)$, so the solution (B22) is used, in which $G_0(\xi) = \Sigma_0(\xi)$ for $-1/v_1 < \xi < -1/v_2$ and vanishes elsewhere. The homogeneous solution for the transform of stress is

$$Y(\zeta) = \frac{S(\zeta; c_s, c_p)(\zeta + 1/c_R)}{(\zeta + 1/v_2)^{3/2}\sqrt{\zeta + 1/c_s}}, \quad \text{(B31)}$$

as in the other semi-infinite crack problem. There is a complication here that arises since the stress field is homogeneous of degree $-1/2$. Noting that equation (B27) may alternatively be written as

$$\sigma_{xy}(x,0,t) = \frac{1}{2\pi^{3/2}\sqrt{x}}\left\{\frac{1}{\sqrt{\xi}} * [\Sigma^+(\xi) - \Sigma^-(\xi)]\right\}_{\xi=-t/x}, \quad \text{(B32)}$$

it is evident that in order for stress to diverge as $(x - v_2 t)^{-1/2}$ at the crack tip, then $\Sigma(\zeta)$ must diverge as $(\zeta + 1/v_2)^{-1}$ rather than as $(\zeta + 1/v_2)^{-3/2}$ as in equation (B23) as $\zeta \to -1/v_2$. To correct this, the homogeneous solution to this problem is taken to be $Y(\zeta)\sqrt{\zeta + 1/v_2}$, with $Y(\zeta)$ still given by equation (B31). As I have been unable to provide a rigorous justification for this correction, an alternative derivation of the solution is presented in Appendix B4.

[99] However, to proceed by the current method, by evaluating the integral in equation (B22), the solution is

$$\Sigma(\zeta) = -\frac{iK\sqrt{v_1}}{\sqrt{2}(1 + v_1\zeta)}\frac{Y(\zeta)\sqrt{\zeta + 1/v_2}}{Y(-1/v_1)\sqrt{-1/v_1 + 1/v_2}}. \quad \text{(B33)}$$

B4. Jump in Rupture Speed: Alternative Solution Using Weiner-Hopf Technique

[100] The solution to the speed-jump problem treated in Appendix B.3 may alternatively be derived using the Weiner-Hopf technique. This approach has been quite successful for semi-infinite crack problems and is well covered by *Freund* [1998, pp. 77–97, 340–350]. The problem will be solved in a frame of reference moving with the crack tip at speed v_2. Any fields in this frame are labeled with a tilde, and the transformation is accomplished by letting $\tilde{x} = x - v_2 t$, $\tilde{y} = y$, and $\tilde{t} = t$. The boundary conditions in this frame are

$$\begin{aligned} \tilde{\sigma}_{xy}(\tilde{x},0,\tilde{t}) &= -\frac{KH[\tilde{x} + (v_2 - v_1)\tilde{t}]}{\sqrt{2\pi[\tilde{x} + (v_2 - v_1)\tilde{t}]}} \quad \text{for } \tilde{x} < 0 \\ \tilde{u}_x(\tilde{x},0^+,\tilde{t}) &= 0 \quad \text{for } \tilde{x} > 0. \end{aligned} \quad \text{(B34)}$$

[101] Transforms in the moving frame are defined as

$$\tilde{F}(\tilde{\zeta}) = \tilde{s}^{n+2}\int_{-\infty}^{\infty} e^{-\tilde{s}\tilde{\zeta}\tilde{x}}\int_0^{\infty} e^{-\tilde{s}\tilde{t}}\tilde{f}(\tilde{x},0,\tilde{t})d\tilde{t}d\tilde{x}. \quad \text{(B35)}$$

and are readily obtained from those in the stationary frame (A1) using the substitutions

$$\tilde{s} = s(1 + v_2\zeta) \quad \text{and} \quad \tilde{\zeta} = \frac{\zeta}{1 + v_2\zeta}, \quad \text{(B36)}$$

and to transform back

$$s = \tilde{s}(1 - v_2\tilde{\zeta}) \quad \text{and} \quad \zeta = \frac{\tilde{\zeta}}{1 - v_2\tilde{\zeta}}. \quad \text{(B37)}$$

The transformed fields are related via

$$\tilde{F}(\tilde{\zeta}) = \frac{F[\tilde{\zeta}/(1 - v_2\tilde{\zeta})]}{(1 - v_2\tilde{\zeta})^{n+2}}, \quad \text{(B38)}$$

from which it follows that the mode-II stress-displacement relationship (B2) becomes

$$\tilde{\Sigma}(\tilde{\zeta}) = -\mu\tilde{B}(\tilde{\zeta})\tilde{U}(\tilde{\zeta}) \quad \text{with} \quad \tilde{B}(\tilde{\zeta}) = \frac{c_s^2\tilde{R}(\tilde{\zeta})}{\tilde{\beta}(\tilde{\zeta})(1-v_2\tilde{\zeta})^2} \tag{B39}$$

and

$$\begin{aligned}\tilde{\alpha}(\tilde{\zeta}) &= (1-v_2\tilde{\zeta})\alpha\left(\frac{\tilde{\zeta}}{1-v_2\tilde{\zeta}}\right)\\ \tilde{\beta}(\tilde{\zeta}) &= (1-v_2\tilde{\zeta})\beta\left(\frac{\tilde{\zeta}}{1-v_2\tilde{\zeta}}\right)\\ \tilde{R}(\tilde{\zeta}) &= (1-v_2\tilde{\zeta})^4 R\left(\frac{\tilde{\zeta}}{1-v_2\tilde{\zeta}}\right).\end{aligned} \tag{B40}$$

The Wiener-Hopf equation is

$$\tilde{\Sigma}^+(\tilde{\zeta}) + \tilde{\Sigma}_0(\tilde{\zeta}) = -\mu\tilde{B}^+(\tilde{\zeta})\tilde{B}^-(\tilde{\zeta})\tilde{U}^-(\tilde{\zeta}), \tag{B41}$$

where $\tilde{\Sigma}_0(\tilde{\zeta})$ is the transform of the known stress for $\tilde{x} < 0$ as given in equation (B34):

$$\tilde{\Sigma}_0(\tilde{\zeta}) = \frac{K}{\sqrt{2}\tilde{\zeta}^{1/2}\left[1-(v_2-v_1)\tilde{\zeta}\right]}, \tag{B42}$$

and the superscripts + and −, in contrast to their previous usage, now indicate functions that are analytic in the half-planes $\mathrm{Re}(\tilde{\zeta}) > -1/(c_p - v_2)$ and $\mathrm{Re}(\tilde{\zeta}) < 1/(c_p + v_2)$. The product factorization of $\tilde{B}(\tilde{\zeta}) = \tilde{B}^+(\tilde{\zeta})\tilde{B}^-(\tilde{\zeta})$ has been obtained, for example, by *Freund* [1998, pp. 345–347]:

$$\tilde{B}^{\pm}(\tilde{\zeta}) = \frac{\kappa^{1/2}c_s}{v_2}\frac{\left[1/(c_R \mp v_2) \pm \tilde{\zeta}\right]\tilde{S}^{\pm}(\tilde{\zeta})}{\tilde{\beta}^{\pm}(\tilde{\zeta})}, \tag{B43}$$

where

$$\begin{aligned}\kappa &= 4\sqrt{1-v_2^2/c_p^2}\sqrt{1-v_2^2/c_s^2} - \left(2-v_2^2/c_s^2\right)^2\\ \tilde{\alpha}^{\pm}(\tilde{\zeta}) &= \sqrt{\tfrac{1-v_2\tilde{\zeta}}{c_p} \pm \tilde{\zeta}}\\ \tilde{\beta}^{\pm}(\tilde{\zeta}) &= \sqrt{\tfrac{1-v_2\tilde{\zeta}}{c_s} \pm \tilde{\zeta}}\\ \tilde{S}^{\pm}(\tilde{\zeta}) &= S\left(\pm\tfrac{\tilde{\zeta}}{1-v_2\tilde{\zeta}}; c_s, c_p\right)/S\left(\mp 1/v_2; c_s, c_p\right),\end{aligned} \tag{B44}$$

where $S(\zeta)$ is defined in equation (B10).

[102] Solution of the Weiner-Hopf equation proceeds by writing equation (B41) as

$$\frac{\tilde{\Sigma}^+(\tilde{\zeta})}{\tilde{B}^+(\tilde{\zeta})} + \frac{\tilde{\Sigma}_0(\tilde{\zeta})}{\tilde{B}^+(\tilde{\zeta})} = -\mu\tilde{B}^-(\tilde{\zeta})\tilde{U}^-(\tilde{\zeta}). \tag{B45}$$

[103] The right-hand side of equation (B45) is analytic in the half-plane $\mathrm{Re}(\tilde{\zeta}) < 1/(c_p + v_2)$, while the left-hand side is analytic in the half-plane $\mathrm{Re}(\tilde{\zeta}) > -1/(c_p - v_2)$ except for a pole at $\tilde{\zeta} = 1/(v_2 - v_1)$ from $\tilde{\Sigma}_0(\tilde{\zeta})$. Adding a term to both sides to set the residue of this pole to zero yields

$$\begin{aligned}&\frac{\tilde{\Sigma}^+(\tilde{\zeta})}{\tilde{B}^+(\tilde{\zeta})} + \frac{K}{\sqrt{2}\left[1-(v_2-v_1)\tilde{\zeta}\right]}\\ &\left\{\frac{1}{\tilde{\zeta}^{1/2}\tilde{B}^+(\tilde{\zeta})} - \frac{1}{[1/(v_2-v_1)]^{1/2}\tilde{B}^+[1/(v_2-v_1)]}\right\}\\ &= -\mu\tilde{B}^-(\tilde{\zeta})\tilde{U}^-(\tilde{\zeta})\\ &-\frac{K}{\sqrt{2}\left[1-(v_2-v_1)\tilde{\zeta}\right]}\frac{1}{[1/(v_2-v_1)]^{1/2}\tilde{B}^+[1/(v_2-v_1)]}.\end{aligned} \tag{B46}$$

Both sides of equation (B46) are analytic in their respective, but overlapping, half-spaces; hence, both sides must be equal to the same entire function (i.e., a polynomial in $\tilde{\zeta}$, which gives homogeneous solutions to the equation). Only the particular solution due to the load is of interest here, so the polynomial is set to zero. The additional stress is then

$$\tilde{\Sigma}^+(\tilde{\zeta}) = \frac{K\sqrt{v_2-v_1}}{\sqrt{2}\left[1-(v_2-v_1)\tilde{\zeta}\right]}\frac{\tilde{B}^+(\tilde{\zeta})}{\tilde{B}^+[1/(v_2-v_1)]}. \tag{B47}$$

Using equation (B43) to convert back to the stationary frame gives

$$\begin{aligned}\Sigma^+(\zeta) = &-\frac{K\sqrt{v_1}(v_2/v_1-1)}{\sqrt{2}(1+v_1\zeta)(1+v_2\zeta)}\\ &\times\frac{(1/c_R+\zeta)S(\zeta;c_s,c_p)\sqrt{1/v_1-1/c_s}}{(1/c_R-1/v_1)S(-1/v_1;c_s,c_p)\sqrt{\zeta+1/c_s}},\end{aligned} \tag{B48}$$

which is identical to the previously derived expression (B33).

Appendix C: Numerical Method and Initial Static Solutions

[104] This appendix describes the numerical procedures used to calculate spontaneous rupture growth. The spontaneous ruptures in sections 3.2 (two-dimensional ruptures) and 4 (three-dimensional ruptures) are nucleated from a preexisting crack satisfying the Dugdale friction law (7) and those in section 5 (two-dimensional ruptures) from preexisting cracks satisfying power law slip-weakening friction (14).

C1. Boundary Integral Equation Method

[105] The spectral boundary integral equation method developed by *Geubelle and Rice* [1995] is used, which has as its basis the relation

$$\tau(x,t) = \tau_0(x,t) - \frac{\mu}{2c_s}V(x,t) + \phi(x,t), \tag{C1}$$

where $\tau_0(x, t)$ is the stress on the fault in the absence of slip, $V(x, t)$ is the slip velocity, and $\phi(x, t)$ is the stress transfer functional, given in general as a convolution over space and time within the past wave cone. The second term on the right-hand side is the radiation-damping response, relating instantaneous changes in stress to those in slip velocity. While written here in its two-dimensional version, a similar relation holds in three dimensions between the two shear stress components and the components of slip. In the

spectral method, the spatial convolution is performed as a product in the Fourier domain. Furthermore, $\phi(x, t)$ is split into the static contribution, dependent only on current slip, and a contribution describing the transient approach to the static limit. The quasi-dynamic formulation is obtained by neglecting this transient contribution but retaining the radiation-damping term. The fully dynamic formulation, retaining all terms, is used in the spontaneous rupture simulations, while the quasi-dynamic version is utilized to obtain static solutions used as initial conditions in the spontaneous case (see below). In all cases, a second-order Runga-Kutta time-stepping procedure is used as introduced in the context of rate-and-state friction by *Lapusta et al.* [2000].

C2. Static Solution in Two Dimensions for Dugdale Friction

[106] Consider first a singular static crack of length $2L_0$, inside of which the stresses have fallen from the remote loading level, τ_0, to the residual strength, τ_r. The stress induced on the fault is singular at the crack tips but may be relaxed to the peak strength, τ_p, by allowing slip in a cohesive zone of length R_0 extending outside of the original crack. R_0 is determined as a function of L_0 and the nondimensional remote loading level relative to the peak and residual strengths, parameterized here as the seismic S ratio.

[107] The Dugdale friction law, as applied here, is

$$\tau(x) = \begin{cases} \tau_p & \text{for } L_0 < |x| < L_0 + R_0 \\ \tau_r & \text{for } |x| < L_0, \end{cases} \tag{C2}$$

where the extent of the cohesive zone is specified in terms of distance along the fault, rather than in terms of slip, although expressions to convert between these quantities are given below. The solution to this problem was derived by *Bilby et al.* [1963], who give the following expression for displacement on the fault:

$$u_x(x, 0^+, 0) = \frac{(1-\nu)(\tau_p - \tau_r)}{\pi\mu}\left[(x + L_0)\operatorname{arccosh}\left|\frac{(L_0+R_0)^2 + L_0 x}{(L_0+R_0)(L_0+x)}\right| - (x - L_0)\operatorname{arccosh}\left|\frac{(L_0+R_0)^2 - L_0 x}{(L_0+R_0)(L_0-x)}\right|\right], \tag{C3}$$

where ν is Poisson's ratio. Evaluating slip at $x = \pm L_0$ gives the weakening displacement

$$d_0 = \frac{4(1-\nu)(\tau_p - \tau_r)}{\pi\mu} L_0 \ln\left(\frac{L_0 + R_0}{L_0}\right). \tag{C4}$$

To ensure that the crack is in static equilibrium, the following condition must be met:

$$\frac{L_0}{L_0 + R_0} = \sin\left[\frac{\pi S}{2(1+S)}\right], \tag{C5}$$

where S is the seismic S ratio. These relationships may be combined to yield an expression for the equilibrium crack length as a function of S:

$$\frac{\mu d_0}{(\tau_p - \tau_r) L_0} = \frac{4(1-\nu)}{\pi} \ln\csc\left[\frac{\pi S}{2(1+S)}\right] \tag{C6}$$

To ensure adequate numerical resolution, L_0 is resolved with 40 grid points. The resolution of the cohesive zone size R_0 decreases with increasing S, ranging from 40 grid points at $S = 0.5$ to about 16 grid points at $S = 1$. A small perturbation in initial stress, 20% of $\tau_0 - \tau_r$, is applied within the preexisting crack to initiate rupture. The perturbation forces the initial crack to extend slightly beyond its equilibrium length, causing it to become dynamically unstable. The transition lengths are nearly insensitive to the perturbation amplitude. As an example, for $S = 0.5$, decreasing the perturbation amplitude by a factor of 4 (to 5% of $\tau_0 - \tau_r$) only altered the location of the transition by 5 grid points while increasing the amount of time the rupture spent in the quasi-static nucleation phase by over 300 time steps. The 20% level offered a reasonable compromise between making the rupture process independent of the initial perturbation and devoting the majority of the computational resources to the dynamic propagation phase of the rupture process. At the smallest values of S (where the transition lengths approach the initial crack lengths), the perturbation amplitude has a larger influence, and it would perhaps have been preferable to use smaller perturbations in this range. However, a constant perturbation amplitude independent of S was used for simplicity.

C3. Static Solution in Three Dimensions for Dugdale Friction

[108] A similar nucleation procedure is applied in three dimensions. Slip is constrained to the x direction, an assumption that decreases memory requirements by a factor of 2 in the boundary integral equation framework. The boundary condition in the transverse direction is consequently $u_z(x, 0^+, z, t) = 0$. The static problem is specified by first applying the boundary condition $\tau(x, z) = \tau_r$ over some area, where $\tau(x, z)$ refers to $\sigma_{xy}(x, 0, z)$. The area is chosen to be elliptical, characterized by semiaxes L_{x0} and L_{z0} in the x and z directions. For a singular crack model (in which slip is allowed only within this area), there result spatially variable stress singularities at the crack edge. In the Dugdale model, these singularities are relaxed by the introduction of a cohesive zone extending some radial distance ahead of original crack edge. The extent of this zone is also spatially variable, such that the resulting values of d_0, obtained by evaluating slip at the edge of the loaded ellipse, depend upon position along the crack edge. Since the numerical simulations of spontaneous ruptures are to be performed with a single value of d_0, the desired static solution is the one for which d_0 is constant around the crack edge. There is no guarantee that this is at all possible for an elliptical crack (such a solution would require perturbing the shape of the original crack), so the weaker constraint of demanding approximately equal values of d_0 in the purely in-plane and purely antiplane directions is enforced instead.

[109] No analytical solution to this static problem exists but is straightforward to obtain a numerical solution. The traction boundary condition $\tau(x, z) = \tau_r$ is imposed within an elliptical region on a fault subject to a remote loading, τ_0. Stresses outside of this region are prevented from exceeding τ_p, which requires slip to occur within a cohesive zone. These conditions are readily enforced within the context of a boundary integral equation framework; the solution is obtained by solving the problem under the quasi-dynamic

Table C1. Static Crack Parameters in Two and Three Dimensions Under the Dugdale Friction Law[a]

S	$\mu d_0/[(\tau_p - \tau_r)L_0]$ (Two-Dimensional)	$\mu d_0/[(\tau_p - \tau_r)\, L_{x0}]$ (Three-Dimensional)
0.2	1.2907	0.3813
0.3	0.9900	0.3019
0.4	0.7973	0.2464
0.5	0.6619	0.2050
0.6	0.5613	0.1727
0.7	0.4836	
0.8	0.4220	
0.9	0.3721	
1.0	0.3310	
1.1	0.2965	

[a]In two dimensions, the fully weakened region within the crack has half-length L_0. In three dimensions, this region is elliptical, having semiaxes L_{x0} and L_{z0} along the coordinate directions. Slip is allowed only in the x direction and $L_{z0}/L_{x0} = 0.7$.

approximation and is deemed to converge to the static solution when the slip velocity becomes negligible. The eccentricity of the loaded ellipse is varied while preserving its area, $\pi L_{x0}\, L_{z0}$, until the inferred values of d_0 in the two coordinate directions are approximately equal. This occurs when $L_{z0}/L_{x0} \approx 0.7$. The value of d_0 thus obtained is the one used in the dynamic simulations, in which ruptures are nucleated from this original static solution by a slight perturbation (as in two dimensions) within the original elliptical region, again 20% of $\tau_0 - \tau_r$. Here the 20% level was necessary to nucleate ruptures in many cases since the chosen value of d_0 was greater than critical over about half of the rupture front. Values of d_0 as a function of S are given in Table C1, which also gives the two-dimensional values. This numerical procedure is verified by performing a similar calculation in two dimensions, which converges toward the known analytical solution upon refinement of the mesh, but only in the limit that the computational domain size becomes much larger than the initial crack length (so that the influence of the periodic replicas becomes vanishingly small). In the three-dimensional dynamic rupture simulations, L_{x0} and L_{z0} are discretized by 40 and 28 points. In comparison to the two-dimensional case, the values of d_0 (and hence the cohesive zone size) are about a factor of 3 smaller in three dimensions. Memory constraints limit the three-dimensional calculations to values of $S \leq 0.6$.

C4. Static Solution in Two Dimensions for Power Law Slip-Weakening Friction

[110] Static crack solutions may also be constructed for slip-weakening laws of an arbitrary form, in this work for power law slip weakening. In this case, the method outlined for the three-dimensional case for the Dugdale law does not carry over, and an alternative method must be used. Again, the code is run in its quasi-dynamic formulation, with the power law slip-weakening friction law applied everywhere outside the region of imposed stress drop ($|x| < L_0$). A constant stress drop is imposed instantaneously within this region, causing stress transfer to the surrounding portions of the fault. The amplitude of the imposed stress drop is chosen to ensure that the end of the fully weakened cohesive zone coincides with the edges of the imposed stress drop region after all waves have passed and slip velocity has dropped to negligible values. The resulting slip distribution was then used in the initial conditions for the fully dynamic models. This method was validated by comparison to the analytical solution for static cracks under the Dugdale friction law.

Appendix D: Elliptical Crack

[111] This appendix summarizes pertinent details of the solution to a self-similarly expanding elliptical crack [*Burridge and Willis*, 1969; *Richards*, 1973; *Willis*, 1973; *Richards*, 1976]. The displacement function, $u_i(x, y, z, t)$, that satisfies the boundary conditions is

$$u_i(x, 0^+, z, t) = v_i^0 H\left(t - \sqrt{x^2/a^2 + z^2/b^2}\right) \times \sqrt{t^2 - x^2/a^2 - z^2/b^2}, \tag{D1}$$

where $2v_i^0$ is the slip velocity at the origin. Laplace transforming time and Fourier transforming along the x and z directions, such that the solution has $\exp(ik_x x + ik_z z + st)$ dependence, yield

$$U_i(s, k_x, k_z) = \frac{4\pi ab}{\left(s^2 + a^2k_x^2 + b^2k_z^2\right)^2}. \tag{D2}$$

[112] Expressions for the shear and dilatational components of all fields are given by *Richards* [1973]. While the Cagniard-de Hoop method, in its three-dimensional formulation, can be used to invert these transforms [*Richards*, 1973], the method of *Willis* [1973] provides a more direct route to the solution. The inversion formula for either the shear or dilatational component of the field, given in the transform domain by $F(k_x, k_y, s)$ and in the physical domain by $f(x, y, z, t)$, is

$$f(x, y, z, t) = \frac{H(t - t_w)}{2\pi^2}\,\mathrm{Re}\int_\phi^{\phi+\pi} \frac{F(-i\Omega_w, \cos\theta, \sin\theta)}{t + iy\Omega_w/\left(\alpha_w(\Omega_w)c_w^2\right)}\, d\theta, \tag{D3}$$

where $\phi = \arctan(z/x)$, $\alpha_w(\Omega) = \sqrt{1 - \Omega^2/c_w^2}$, and $t_w = y/c_w$ for $w = p$ or s. The Cagniard path is given in terms of the complex along-fault phase velocity of the particular wave type:

$$\Omega_w = \frac{tr\cos(\theta - \phi) + iy\sqrt{t^2 - (r^2\cos^2(\theta - \phi) + y^2)/c_w^2}}{t^2 - y^2/c_w^2}, \tag{D4}$$

which satisfies $\Omega_w t = r\cos(\theta - \phi) + i\alpha_w(\Omega_w)z$, where $r = \sqrt{x^2 + z^2}$. The branch of $\alpha_w(\Omega)$ is chosen such that $\mathrm{Im}[\alpha_w(\Omega)] \geq 0$; the branch cut lies on the real Ω axis between $-c_w$ and c_w. The method is discussed in more detail by *Ren et al.* [2002] and *Dunham* [2005].

[113] The method requires one numerical integration over the variable θ to obtain stress rate and a second over time t to reach stress. Following the strategy suggested by *Willis* [1973, p. 29], the order of integration is switched, and the t integral is converted into one over Ω_w. Furthermore, to avoid singularities in the integrand associated with the rupture front, the θ integral is deformed into the complex

plane using the parameterization $\theta(s) = \phi + s - i \sin s$ for s running between 0 and π. An alternative procedure would be to explicitly subtract the singularity as *Richards* [1973] has done.

[114] **Acknowledgments.** The central ideas and early work for this project occurred at the Kavli Institute for Theoretical Physics during a program on Friction, Fracture, and Earthquake Physics. Support is gratefully acknowledged from a Reginald A. Daly Postdoctoral Fellowship at Harvard and from the NSF/USGS Southern California Earthquake Center, funded by NSF Cooperative Agreement EAR-0106924 and USGS Cooperative Agreement 02HQAG0008. This is SCEC contribution 1007. I thank Ralph Archuleta for the discussions on the practical need for predicting supershear transition lengths, Stefan Nielsen for sharing his solution for the mode-II self-similar rupture pulse, and Jim Rice for the many insightful discussions and in particular for the suggestion to adopt the Dugdale model in seeking analytical confirmation of these theories. The suggestions of Allan Rubin and an anonymous reviewer are most appreciated.

References

Aagaard, B. T., and T. H. Heaton (2004), Near-source ground motions from simulations of sustained intersonic and supersonic fault ruptures, *Bull. Seismol. Soc. Am.*, *94*(6), 2064–2078, doi:10.1785/0120030249.

Aagaard, B. T., T. H. Heaton, and J. F. Hall (2001), Dynamic earthquake ruptures in the presence of lithostatic normal stresses: Implications for friction models and heat production, *Bull. Seismol. Soc. Am.*, *91*(6), 1765–1796.

Abercrombie, R. E., and J. R. Rice (2005), Can observations of earthquake scaling constrain slip weakening?, *Geophys. J. Int.*, *162*, 406–424, doi:10.1111/j.1365-246X.2005.02579.x.

Abraham, F. F., and H. Gao (2000), How fast can cracks propagate?, *Phys. Rev. Lett.*, *84*(14), 3113–3116, doi:10.1103/PhysRevLett.84.311.

Achenbach, J. D., and J. G. Harris (1978), Ray method for elastodynamic radiation from a slip zone of arbitrary shape, *J. Geophys. Res.*, *83*, 2283–2291.

Aki, K., and P. Richards (2002), *Quantitative Seismology*, University Science Books, Sausalito, California.

Andrews, D. J. (1976), Rupture velocity of plane strain shear cracks, *J. Geophys. Res.*, *81*, 5679–5687.

Andrews, D. J. (1985), Dynamic plane-strain shear rupture with a slip-weakening friction law calculated by a boundary integral method, *Bull. Seismol. Soc. Am.*, *75*(1), 1–21.

Antipov, Y. A., O. Obrezanova, and J. R. Willis (2004), A fracture criterion of "Barenblatt" type for an intersonic shear crack, *Math. Mech. Solids*, *9*(3), 271–283, doi:10.1177/1081286504038457.

Archuleta, R. J. (1984), A faulting model for the 1979 Imperial Valley earthquake, *J. Geophys. Res.*, *89*, 4559–4585.

Barenblatt, G. I. (1962), Mathematical theory of equilibrium cracks, *Adv. Appl. Mech.*, *7*, 56–129.

Bernard, P., and D. Baumont (2005), Shear Mach wave characterization for kinematic fault rupture models with constant supershear rupture velocity, *Geophys. J. Int.*, *162*(2), 431–447, doi:10.1111/j.1365-246X.2005.02611.x.

Bhat, H. S., R. Dmowska, G. C. P. King, Y. Klinger, and J. R. Rice (2007), Off-fault damage patterns due to supershear ruptures with application to the 2001 Mw 8.1 Kokoxili (Kunlun) Tibet earthquake, *J. Geophys. Res.*, *112*, B06301, doi:10.1029/2006JB004425.

Bilby, B. A., A. H. Cottrell, and K. H. Swinden (1963), The spread of plastic yield from a notch, *Proc. R. Soc. London Ser. A*, *272*(1350), 304–314.

Bouchon, M., and M. Vallée (2003), Observation of long supershear rupture during the magnitude 8.1 Kunlunshan earthquake, *Science*, *301*, 824–826, doi:10.1126/science.1086832.

Bouchon, M., M. N. Toksöz, H. Karabulut, M.-P. Bouin, M. Dietrich, M. Aktar, and M. Edie (2000), Seismic imaging of the 1999 Izmit (Turkey) rupture inferred from the near-fault recordings, *Geophys. Res. Lett.*, *27*(18), 3013–3016, doi:10.1029/2000GL011761.

Bouchon, M., M.-P. Bouin, H. Karabulut, M. N. Toksöz, M. Dietrich, and A. J. Rosakis (2001), How fast is rupture during an earthquake? New insights from the 1999 Turkey earthquakes, *Geophys. Res. Lett.*, *28*, 2723–2726, doi:10.1029/2001GL013112.

Bouchon, M., M. N. Toksöz, H. Karabulut, M.-P. Bouin, M. Dietrich, M. Aktar, and M. Edie (2002), Space and time evolution of rupture and faulting during the 1999 Izmit (Turkey) earthquake, *Bull. Seismol. Soc. Am.*, *92*(1), 256–266, doi:10.1785/0120000845.

Broberg, K. B. (1994), Intersonic bilateral slip, *Geophys. J. Int.*, *119*, 706–714.

Broberg, K. B. (1995), Intersonic mode II crack expansion, *Arch. Mech.*, *47*, 859–871.

Broberg, K. B. (1999a), *Cracks and Fracture*, Elsevier, New York..

Broberg, K. B. (1999b), Intersonic mode II crack acceleration, *Fatigue Fract. Eng. Mater. Struct.*, *22*, 17–24.

Burridge, R. (1973), Admissible speeds for plane-strain shear cracks with friction but lacking cohesion, *Geophys. J. R. Astron. Soc.*, *35*, 439–455.

Burridge, R., and J. R. Willis (1969), The self-similar problem of the expanding elliptical crack in an anisotropic solid, *Proc. Camb. Philol. Soc.*, *66*, 443–468.

Burridge, R., G. Conn, and L. B. Freund (1979), The stability of a rapid mode II shear crack with finite cohesive traction, *J. Geophys. Res.*, *85*, 2210–2222.

Campillo, M., and I. R. Ionescu (1997), Initiation of antiplane shear instability under slip dependent friction, *J. Geophys. Res.*, *102*(B9), 20,363–20,371.

Das, S., and K. Aki (1977), A numerical study of two-dimensional spontaneous rupture propagation, *Geophys. J. R. Astron. Soc.*, *50*, 643–668.

Day, S. M. (1982a), Three-dimensional finite difference simulation of fault dynamics: Rectangular faults with fixed rupture velocity, *Bull. Seismol. Soc. Am.*, *72*, 705–727.

Day, S. M. (1982b), Three-dimensional simulation of spontaneous rupture: The effect of nonuniform prestress, *Bull. Seismol. Soc. Am.*, *72*, 1881–1902.

Dugdale, D. S. (1960), Yielding of steel sheets containing slits, *J. Mech. Phys. Solids*, *8*, 100–104.

Dunham, E. M. (2005), Dissipative interface waves and the transient response of a three-dimensional sliding interface with Coulomb friction, *J. Mech. Phys. Solids*, *53*(2), 327–357, doi:10.1016/j.jmps.2004.07.003.

Dunham, E. M., and R. J. Archuleta (2004), Evidence for a supershear transient during the 2002 Denali Fault earthquake, *Bull. Seismol. Soc. Am.*, *94*(6B), S256–S268, doi:10.1785/0120040616.

Dunham, E. M., and R. J. Archuleta (2005), Near-source ground motion from steady state dynamic rupture pulses, *Geophys. Res. Lett.*, *32*, L03302, doi:10.1029/2004GL021793.

Dunham, E. M., P. Favreau, and J. M. Carlson (2003), A supershear transition mechanism for cracks, *Science*, *299*, 1557–1559.

Ellsworth, W. L., et al. (2004), Near-field ground motion of the 2002 Denali Fault, Alaska, earthquake recorded at Pump Station 10, *Earthq. Spectra*, *20*(3), 597–615, doi:10.1193/1.1778172.

Eshelby, J. D. (1969), The elastic field of a crack extending non-uniformly under general antiplane loading, *J. Mech. Phys. Solids*, *17*, 177–199.

Favreau, P., M. Campillo, and I. R. Ionescu (1999), Initiation of in-plane shear instability under slip-dependent friction, *Bull. Seismol. Soc. Am.*, *89*, 1280–1295.

Favreau, P., M. Campillo, and I. R. Ionescu (2002), Initiation of shear instability in three-dimensional elastodynamics, *J. Geophys. Res.*, *107*, (B7), 2147, doi:10.1029/2001JB000448.

Fossum, A. F., and L. B. Freund (1975), Nonuniformly moving shear crack model of a shallow focus earthquake mechanism, *J. Geophys. Res.*, *80*, 3343–3347.

Freund, L. B. (1972a), Crack propagation in an elastic solid subjected to general loading: I. Constant rate of extension, *J. Mech. Phys. Solids*, *20*, 129–140.

Freund, L. B. (1972b), Crack propagation in an elastic solid subjected to general loading: II. Non-uniform rate of extension, *J. Mech. Phys. Solids*, *20*, 141–152.

Freund, L. B. (1998), *Dynamic Fracture Mechanics*, Cambridge Univ. Press, New York.

Fukuyama, E., and K. B. Olsen (2002), A condition for super-shear rupture propagation in a heterogeneous stress field, *Pure Appl. Geophys.*, *157*, 2047–2056.

Gao, H., Y. Huang, and F. F. Abraham (2001), Continuum and atomistic studies of intersonic crack propagation, *J. Mech. Phys. Solids*, *49*, 2113–2132.

Geubelle, P. H., and J. R. Rice (1995), A spectral method for three-dimensional elastodynamic fracture problems, *J. Mech. Phys. Solids*, *43*, 1791–1824.

Gonzalez, S. (2003), Foam rubber and numerical simulations of near-fault seismic directivity, Master's thesis, San Diego State Univ., San Diego, Calif..

Guatteri, M., and P. Spudich (2000), What can strong-motion data tell us about slip-weakening fault-friction laws, *Bull. Seismol. Soc. Am.*, *90*(1), 98–116, doi:10.1785/0119990053.

Guo, G., W. Yang, and Y. Huang (2003a), Intersonic crack growth under time-dependent loading, *Int. J. Solids Struct.*, *40*(11), 2757–2765, doi:10.1016/S0020-7683(03)00085-4.

Guo, G., W. Yang, Y. Huang, and A. J. Rosakis (2003b), Sudden deceleration or acceleration of an intersonic shear crack, *J. Mech. Phys. Solids*, *51*, 311–331.

Huang, Y., and H. Gao (2001), Intersonic crack propagation: Part I. The fundamental solution, *J. Appl. Mech.*, *68*, 169–175.
Huang, Y., and H. Gao (2002), Intersonic crack propagation: Part II. Suddenly stopping crack, *J. Appl. Mech.*, *69*, 76–80.
Kostrov, B. V. (1966), Unsteady propagation of longitudinal shear cracks, *J. Appl. Math. Mech.*, *30*, 1241–1248.
Kostrov, B. V. (1975), On the crack propagation with variable velocity, *Int. J. Fract.*, *11*, 47–56.
Lapusta, N., J. R. Rice, Y. Ben-Zion, and G. Zheng (2000), Elastodynamic analysis for slow tectonic loading with spontaneous rupture episodes on faults with rate- and state-dependent friction, *J. Geophys. Res.*, *105*(B10), 23,765–23,790, doi:10.1029/2000JB900250.
Madariaga, R. (1977), High-frequency radiation from crack (stress drop) models of earthquake faulting, *Geophys. J. R. Astron. Soc.*, *51*, 625–651.
Madariaga, R., and K. B. Olsen (2000), Criticality of rupture dynamics in 3-D, *Pure Appl. Geophys.*, *157*, 1981–2001.
Madariaga, R., S. Peyrat, and K. B. Olsen (2000), Rupture dynamics in 3D: A review, in *Problems in Geophysics for the New Millennium*, edited by E. Boschi, G. Ekström, and A. Morelli, Editrice Compositori, Bologna, Italy.
Muskhelishvili, N. I. (1953), *Singular Integral Equations: Boundary Problems of Function Theory and Their Application to Mathematical Physics*, translated from Russian edited by J. R. M. Radok, Springer, New York.
Needleman, A. (1999), An analysis of intersonic crack growth under shear loading, *J. Appl. Mech.*, *66*(4), 847–857.
Nielsen, S., and R. Madariaga (2003), On the self-healing fracture mode, *Bull. Seismol. Soc. Am.*, *93*(6), 2375–2388, doi:10.1785/0120020090.
Obrezanova, O., and J. R. Willis (2003), Stability of intersonic shear crack propagation, *J. Mech. Phys. Solids*, *51*(11), 1957–1970, doi:10.1016/j.jmps.2003.09.008.
Olsen, K. B., R. Madariaga, and R. J. Archuleta (1997), Three-dimensional dynamic simulation of the 1992 Landers earthquake, *Science*, *278*, 834–838.
Pao, Y.-H., and R. R. Gajewski (1977), The generalized ray theory and transient responses of layered elastic solids, in *Physical Acoustics*, vol. 13, edited by W. P. Mason and R. N. Thurston, pp. 183–265, Springer, New York.
Ren, S., N. N. Hsu, and D. G. Eitzen (2002), Transient Green's tensor for a layered solid half-space with different interface conditions, *J. Res. Natl. Inst. Stand. Technol.*, *107*(5), 445–473.
Rice, J. R. (2006), Heating and weakening of faults during earthquake slip, *J. Geophys. Res.*, *111*(B5), B05311, doi:10.1029/2005JB004006.
Rice, J. R., and K. Uenishi (2002), Slip development and instability on a heterogeneously loaded fault with power-law slip-weakening, *Eos Trans. AGU*, *83*(47), Fall Meet. Suppl., Abstract S42H-08.
Richards, P. G. (1973), The dynamic field of a growing plane elliptical shear crack, *Int. J. Solids Struct.*, *9*, 843–861.
Richards, P. G. (1976), Dynamic motions near an earthquake fault: A three-dimensional solution, *Bull. Seismol. Soc. Am.*, *66*, 1–32.
Rosakis, A. J., O. Samudrala, and D. Coker (1999), Cracks faster than the shear wave speed, *Science*, *284*, 1337–1340.
Rose, L. R. F. (1981), The stress-wave radiation from growing cracks, *Int. J. Fract.*, *17*(1), 45–60.
Somerville, P. G., N. F. Smith, R. W. Graves, and N. A. Abrahamson (1997), Modification of empirical strong ground motion attenuation relations to include the amplitude and duration effects of rupture directivity, *Seismol. Res. Lett.*, *68*, 199–222.
Spudich, P., and E. Cranswick (1984), Direct observation of rupture propagation during the 1979 Imperial Valley earthquake using a short baseline accelerometer array, *Bull. Seismol. Soc. Am.*, *74*(6), 2083–2114.
Spudich, P., B. S. J. Chiou, R. Graves, N. Collins, and P. Somerville (2004), A formulation of directivity for earthquake sources using isochrone theory, *U.S. Geol Surv. Open File Rep., 2004–1268*.
Uenishi, K., and J. R. Rice (2003), Universal nucleation length for slip-weakening rupture instability under nonuniform fault loading, *J. Geophys. Res.*, *108*(B1), 2042, doi:10.1029/2001JB001681.
Uenishi, K., and J. R. Rice (2004), Three-dimensional rupture instability of a slip-weakening fault under heterogeneous loading, *Eos Trans. AGU*, *85*(47), Fall Meet. Suppl., Abstract S13E-04.
Willis, J. R. (1973), Self-similar problems in elastodynamics, *Phil. Trans. R. Soc. London Ser. A*, *247*, 435–491.
Xia, K., A. J. Rosakis, and H. Kanamori (2004), Laboratory earthquakes: The sub-Rayleigh-to-supershear transition, *Science*, *303*(5665), 1859–1861, doi:10.1126/science.1094022.

E. M. Dunham, Department of Earth and Planetary Sciences, Harvard University, 20 Oxford St., Cambridge, MA 02138, USA. (edunham@fas.harvard.edu)